Angewandte Chemie
Eine Zeitschrift der Gesellschaft Deutscher Chemiker

Supporting Information

Mechanocatalytic Room-Temperature Synthesis of Ammonia from Its Elements Down to Atmospheric Pressure

*Steffen Reichle, Michael Felderhoff, and Ferdi Schüth**

anie_202112095_sm_miscellaneous_information.pdf

SUPPORTING INFORMATION

Table of Contents

Materials and Methods

S1. Materials

All chemicals were received from commercial suppliers and were used as received, unless noted otherwise: Al (Alfa Aesar, 99.5 %), Al_2O_3 (Riedel-de-Haën, min. 98 %), Ba (Sigma-Aldrich, > 99 %), BN (Sigma Aldrich, 98 %), Ca (Alfa Aesar, redistilled), CaF_2 (Riedel-de-Haën, min. 99.5 %), CaH_2 (Strem Chemicals, min. 97 %), Co (Sigma-Aldrich, 99.9+ %), Cs (Alfa Aesar, 99.98 %), Cs_2CO_3 (Sigma-Aldrich, 99 %), $CsNO_3$ (Alfa Aesar, 99.99 %), $CsOH{\cdot}H_2O$ (Sigma Aldrich, 99.95 %, treated for 5 h at 280 °C under vacuum before use, see fig. S1 for PXRD), Fe (Sigma-Aldrich, ≥ 99.5 %), Fe_2O_3 (Riedel-de-Haën, min. 97 %), Fe_3O_4 (Alfa Aesar, 97 %), K (Alfa Aesar, 99.95 %), K_2CO_3 (Alfa Aesar, 99 %), KNO_3 (Fluka, > 99.0 %), Li (Sigma-Aldrich, 99 %), LiH (Sigma Aldrich, 95 %), Li_3N (Sigma Aldrich, 80 mesh), Li_2O (Alfa Aesar, 99.5 %), $LiFeO_2$ (Sigma-Aldrich, 95 %), MgO (Sigma-Aldrich, ≥ 99 %, treated for 3 h at 300 °C under vacuum before use), Mn (Alfa Aesar, 99.95 %), Mo (Alfa Aesar, 99.9 %), Na (Sigma-Aldrich, 99.95 %), NaH (Sigma Aldrich, 90 %), Ni (Alfa Aesar, 99.8 %), Rb (Strem Chemicals, 99.9 %), Ru (Alfa Aesar, 99.9 %), $Ru@Al_2O_3$ (Alfa Aesar, 5 % Ru), Ti (Alfa Aesar, 99.5 %), TiN (Alfa Aesar, 99.7 %), TiO_2 (Fluka, > 99 %).

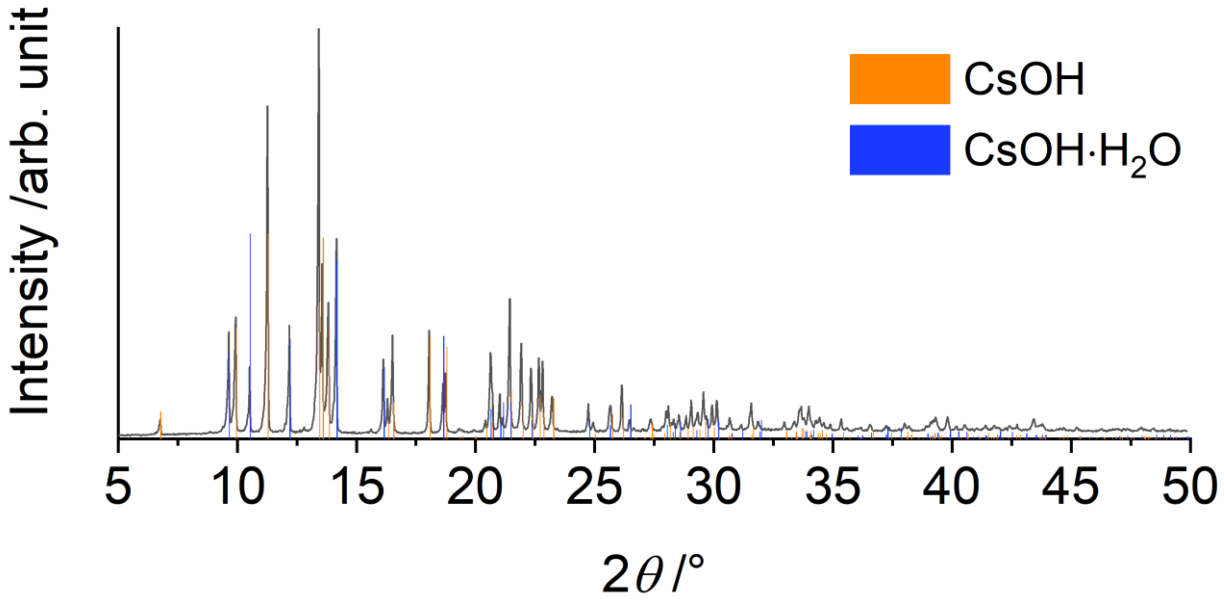

Fig. S1: PXRD of the $CsOH \cdot x\ H_2O$ used herein. It can be seen, that the thermal treatment of $CsOH \cdot H_2O$ led to partial dehydration.

All common gases were received from Air Liquide. For the batch reactions, normally a H_2:N_2 (3:1) gas mixture was used (25 vol% nitrogen (N50), rest hydrogen (N30)). For certain reactions, a H_2:N_2 (1:1) mixture was used, that was prepared in-house. For the continuous reactions, gases were mixed individually from the pure gases (nitrogen 99.9999 %, hydrogen 99.9999 %). The reaction gases were additionally purified by Oxiclear gas-purification columns (LTP-Edelgase). The gases used for calibration of the IR-spectrometers were a mixture of ammonia (2000 ppm) in nitrogen as well as a mixture of 5 vol% ammonia in nitrogen and hydrogen (20 vol% nitrogen, rest hydrogen). $^{15}N_2$ was received from Sigma-Aldrich (98 atom% ^{15}N).

All chemicals were handled in an MBRAUN Labmaster glovebox with levels of oxygen and water ≤ 1 ppm.

Alkali metal ferrites $AFeO_2$ (A = K, Cs) were synthesized according to the literature with slight adaptions.[1] Under inert atmosphere, a total of 5 g of a 1:1 mixture (molar ratio) of Fe_2O_3 and A_2CO_3 (A = K, Cs) was thoroughly ground in an agate mortar and filled in a ceramic crucible. Under argon, the mixture was heated at 5 K/min to 900 °C, kept at 900 °C for 24 h and cooled down with the natural cooling rate of the oven. The product was transferred and kept in a glovebox. All starting materials were subjected to heat treatment (4 h at 300 °C under vacuum) prior to the synthesis to remove water. PXRDs of the alkali ferrites used can be found in figure S2.

Lithium was used in the form of lithium sand, which was kindly provided by Dr. Alexander Bodach and Frederick Winkelmann. It was synthesized according to a modified procedure of Rapoport *et al.* [2]

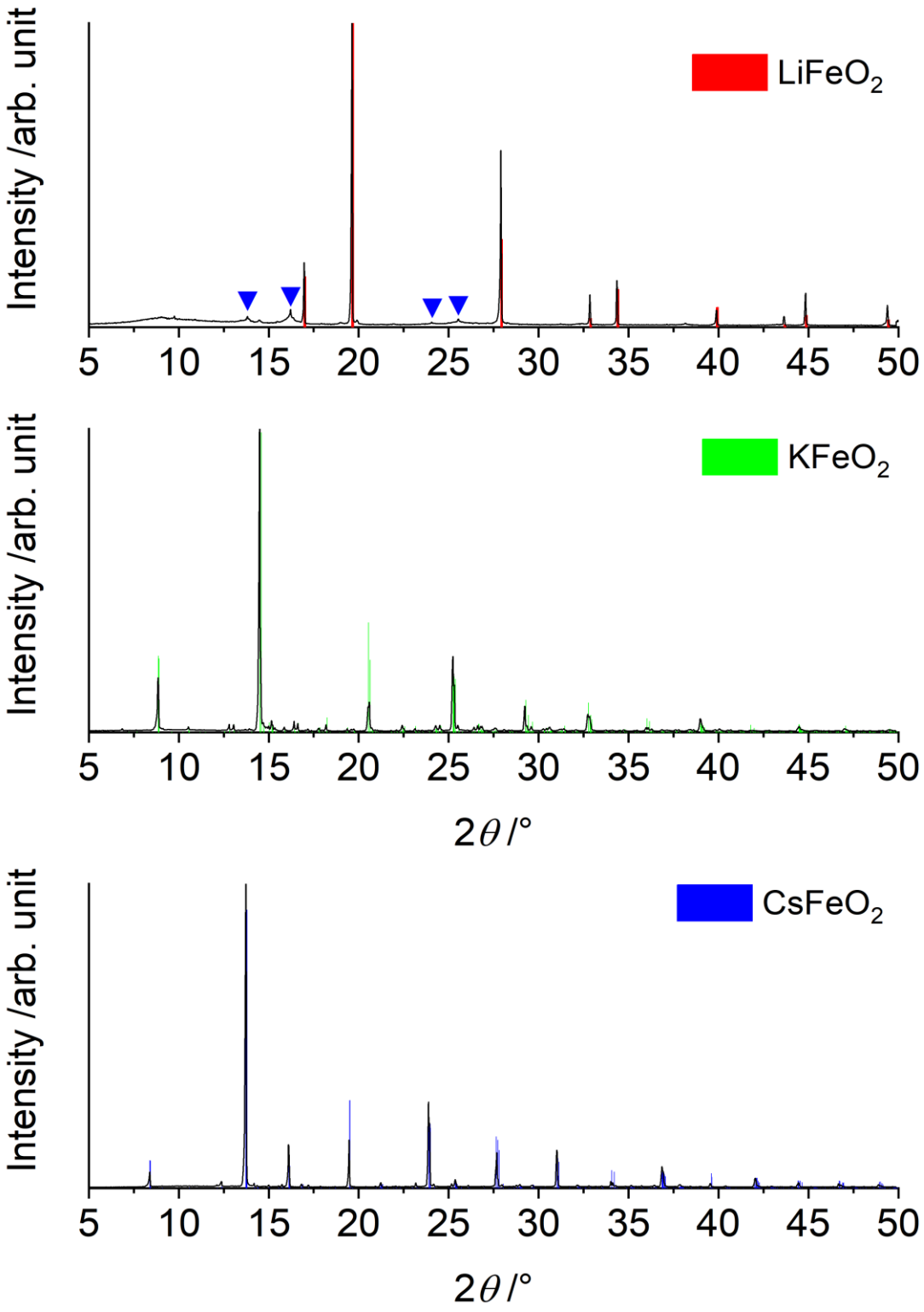

Fig. S2: PXRDs of the alkali ferrites used in this work. The ferrites of potassium and cesium were synthesized as phase pure solids, whereas the PXRD of the commercial $LiFeO_2$ shows additional reflections of $LiFe_5O_8$ (▼).

S2. Procedures for the mechanocatalytic reactions

Batch reactions:

The batch reactions were performed using a pressurizable home-built milling jar made from steel (type 1.4571), equipped with a Teflon-lid to prevent powder from leaving the milling chamber. This Teflon-lid was covered with a punched steel cap at its bottom in order to prevent the balls from directly hitting the Teflon, as well as with a metal frit (2 μm, VA steel) on the top to guarantee for gas in- and outlet while retaining the powder (see fig. S3 and S4 for pictures and description). In all experiments, the jar was loaded with three stainless steel balls having a diameter of 10 mm and three stainless steel balls having a diameter of 15 mm before the chemicals were filled into the jar inside a glovebox. The milling chamber was covered with the Teflon-lid before the actual lid was used to close the jar, being tightened with a torque wrench (20 Nm). Outside the glovebox, the jar was pressurized with the gas mixture to a certain pressure and then subjected to the milling process inside a Fritsch Pulverisette 6. Each experiment consisted of multiples of 30 min runs to reach the total milling time, with a pause of 5 min in between each run to allow for cooling. After the experiment, the gas phase was released into a 600 ml gas sampling bag (Supel, Inert Multi-Layer Foil), out of which it was pushed into the gas cell of the infrared-spectrometer (see text S4). The jar with the remaining powder was transferred into a glovebox, where the product was stored for further analysis. The volume of the jar including the Teflon-lid was determined to be 39.1 ml (see text S3).

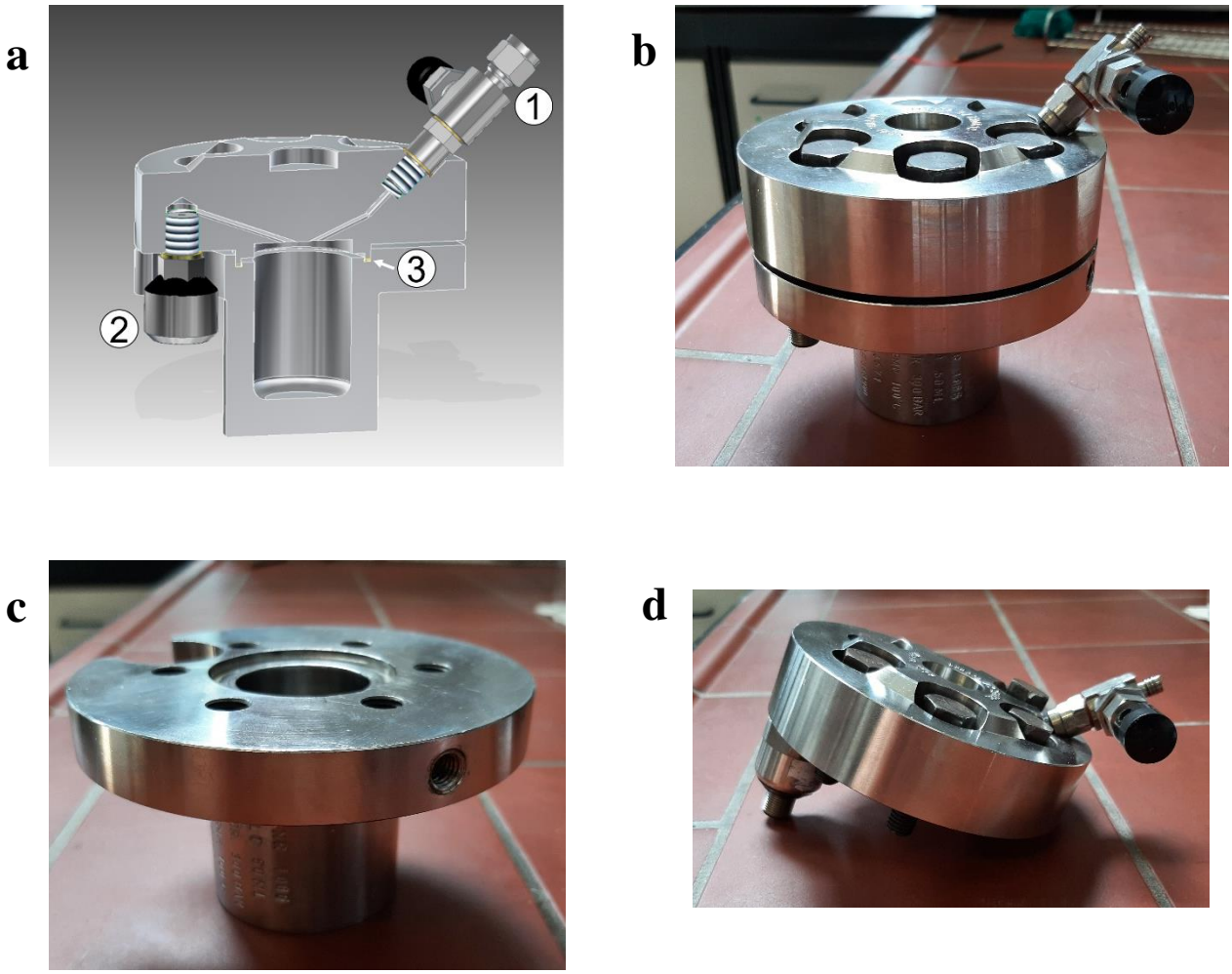

Fig. S3: Drawing and picture of the milling jar used for the batch experiments. a) Technical drawing (cross-section) of the jar with gas connection (1), pressure transducer (2) and PEEK sealing (3). b) Image of the jar completely assembled. c) Side-view image of the bottom part of the jar. d) Side-view onto the lid.

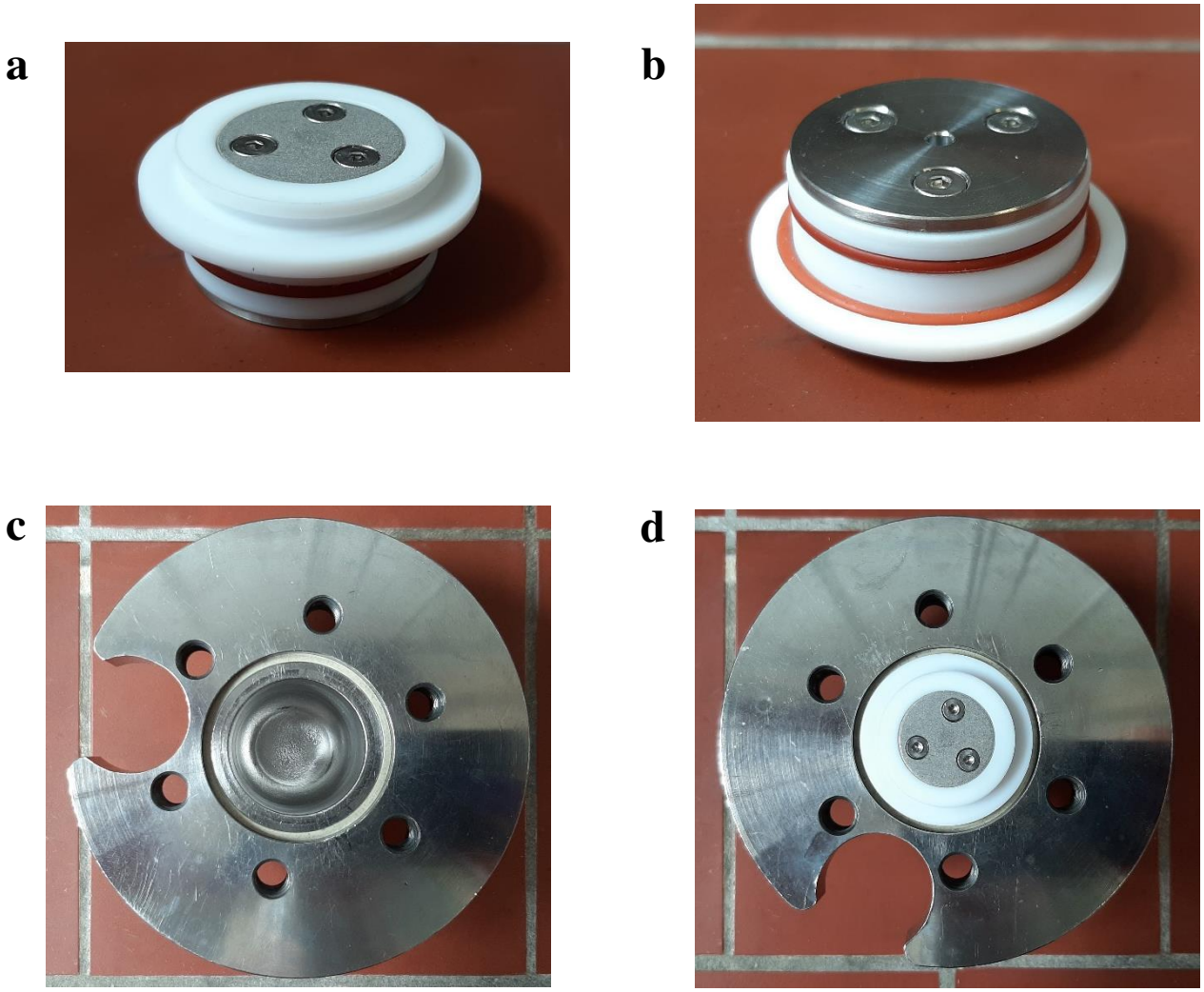

Fig. S4: Images of the Teflon-lid and its assembly into the jar. a) View onto the top part of the Teflon-lid, showing the metal frit. b) View onto the bottom part of the Teflon-lid, showing the punched steel cap and rubber sealing to avoid loss of powder over the edges. c) Empty jar without Teflon-lid. d) Teflon-lid inserted into the jar.

Continuous-flow experiments:

The continuous-flow experiments were performed on a home-built set-up, depicted in fig. S5 A Retsch MM400 shaker mill and pressurizable, home-built jars with a volume of 23 ml were used for the experiments. For more details on the jars used herein, please refer to the explanations connected to figures S6 and S7. In the beginning of the project, the jar contained two metal frits, one at the gas-inlet and one at the top of the funnel (see fig. S6 and S7). After preliminary experiments it was found, that a lot of powder (> 50 %) was stuck in the funnel, which originally was envisaged to act as a kind of cyclone filter, ensuring back-flow of the powder into the jar. Since this idea was shown to not work for the ammonia mechanocatalysts, possibly due to the extensive milling times and the elevated pressure, a third, additional frit was inserted into the bottom of the jar (see fig. S6). This additional frit had a hole in the middle to allow the thermocouple to pass through. This additional frit has proven suitable of keeping all the powder inside the jar, without creating a measurable pressure drop (see table S5 for reactions with and without this additional frit, the higher observed ammonia formation is due to the higher amounts of powder retained in the jar during milling). In a typical experiment, the jar, which already had all the gas connections (end closed by needle-valves) and the thermocouple connected, was loaded inside a glovebox with two stainless steel balls (15 mm diameter) before the chemicals were filled in. The jar was closed tightly and transferred to the set-up. There, the gas-inlet connection of the jar (with closed needle-valve) was first pressurized to around 10 bar with H_2:N_2 (3:1) and the gas was released to the atmosphere. This procedure was performed three times to exclude air trapped in this connection. After that, the needle-valve at the gas-inlet side was opened and the jar was slightly pressurized. Then the needle-valve at the gas-outlet side was opened to remove air trapped in the tubing after this connection and then the jar was flushed first at 20 ml/min (STP) with H_2:N_2 (3:1) at room-temperature for 30 min, before a background spectrum was taken for the infrared measurements. Subsequently, the jar was pressurized to a certain pressure by closing the back-pressure regulator, and the milling experiment was started after the desired pressure was reached. For experiments with external cooling, this was also the start of cooling with a flow of pre-cooled nitrogen gas from the outside. Due to safety reasons the milling could only be performed during the day, so for experiments that required more time, the valves at the connections to the jar were closed at the end of the day, the gas flow and the mill were stopped and the gas fed into the infrared spectrometer was changed to nitrogen overnight. The next day, the experiment was continued by opening all connections to the jar again, the gas-flow into the spectrometer was switched back to the product gas of the experiment, the mill as well as the external cooling was switched on again at the previous settings. This stop and restart method also leads to the downward spikes visible in all curves of ammonia formation over time, since the infrared spectrometer is refilled with the product gas only after a certain time and the jar loses about 4 bar of pressure overnight, which have to be compensated the next day and lead to dilution of the ammonia in the remaining gas phase inside the jar.

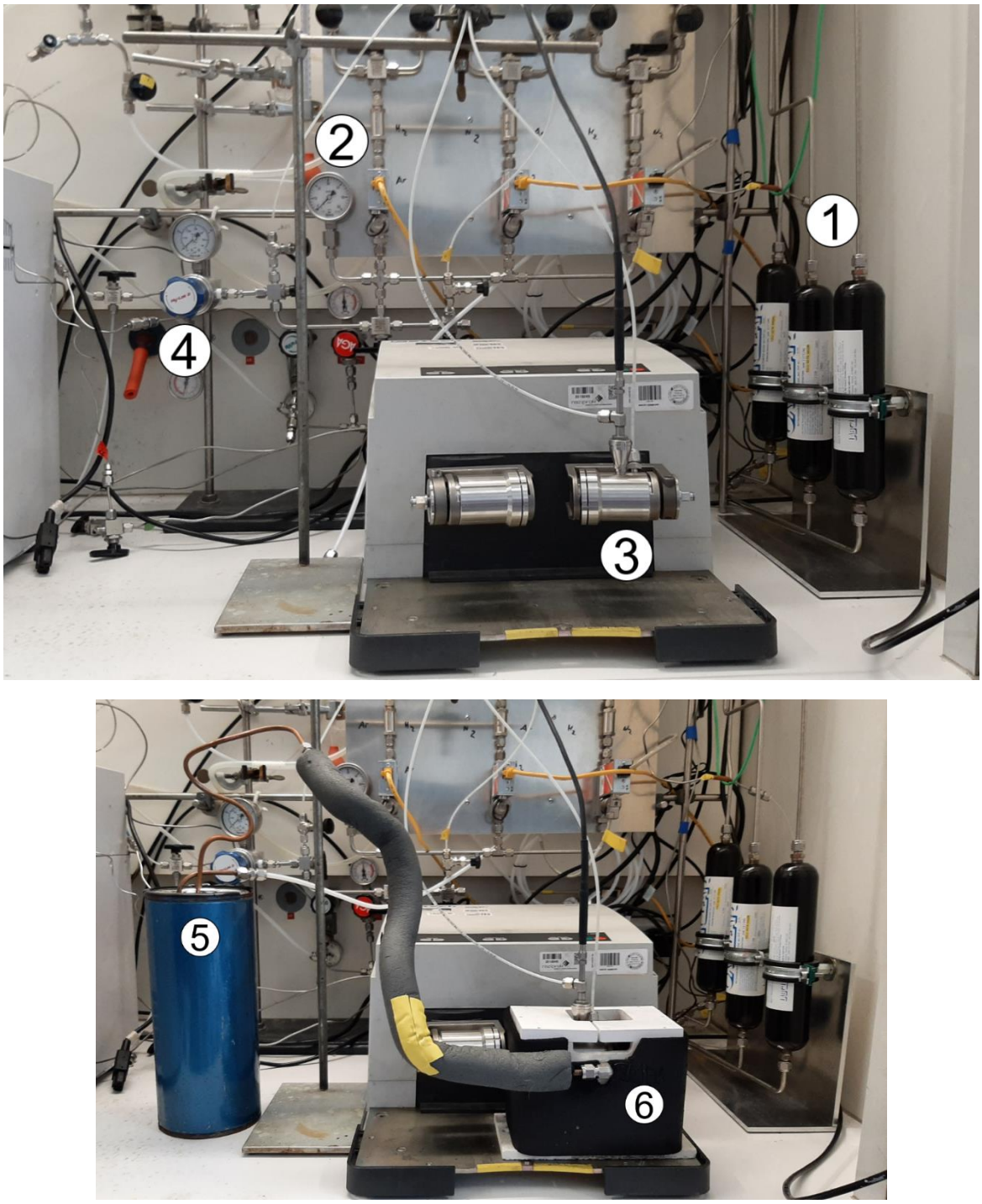

Fig. S5: Set-Up for the continuous mechanocatalytic ammonia synthesis. Inlets of individual gases, additionally purified by Oxiclear gas-purification columns (LTP-Edelgase) (1). Dosing of gases using mass-flow-controllers (Bronkhorst), manometer (2). Modified Retsch MM400 shaker mill with home-built jar equipped with thermocouple and gas connections (3). Back-pressure regulator (Hy-Lok) (4). Dewar with copper spiral for cooling down nitrogen gas in order to control the average temperature of the milling jar (5) and cooling-box made out of fiberglass sheets (6). The cooling system (as well as a heating system) was described previously.[3]

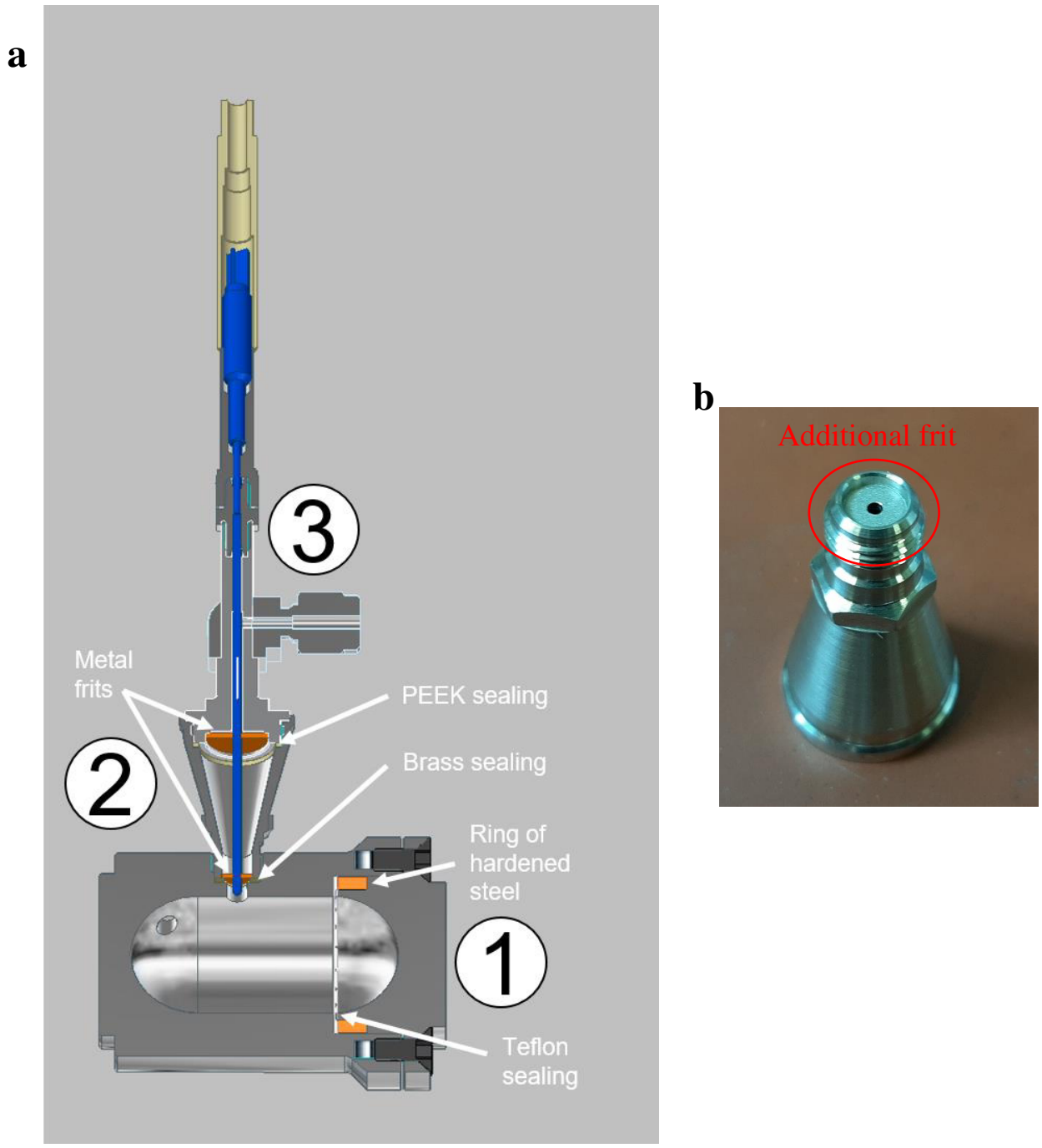

Fig. S6: Details of the home-built pressurizable milling jar. a) Technical drawing (cross-section) of the jar, showing the lid (1) with a ring of hardened steel and a Teflon sealing, the funnel (2) holding the thermocouple and metal frits as well as sealing made from brass or PEEK, the thermocouple with gas outlet (3). b) Picture of the bottom of the funnel with the additional metal frit to avoid powder loss. The hole in the middle allows pass-through of the thermocouple. All frits used herein had a pore size of 2 μm and were made of VA steel.

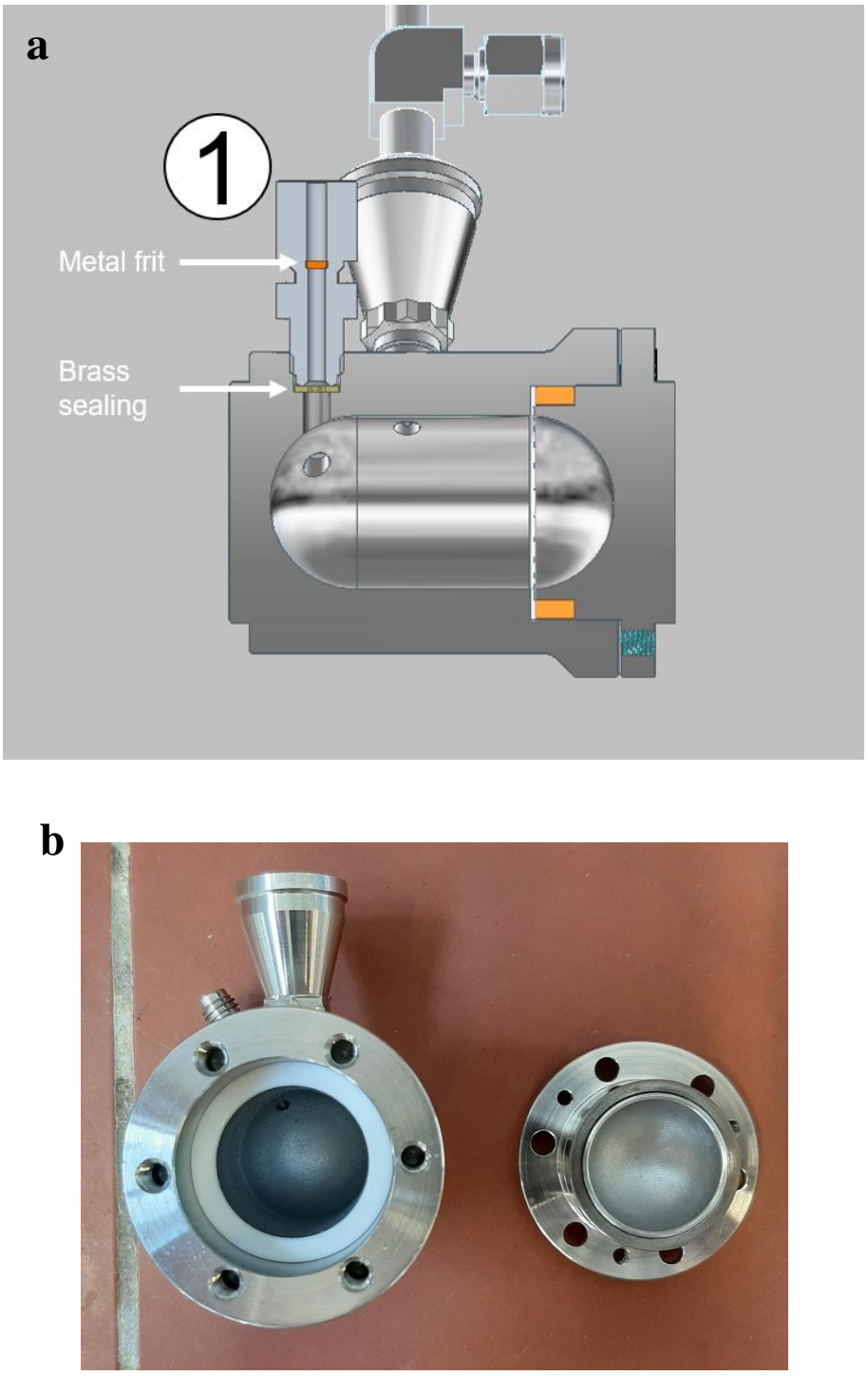

Fig. S7: Further details of the home-built pressurizable milling jar. a) Technical drawing (cross section) of the jar, showing the gas inlet (1) with brass sealing and metal frit. b) Picture of the jar, body (left) and lid (right).

S3. Determination of the milling jar volume

The volume of the jars used for the continuous flow experiments was determined from the technical drawing, which was the basis for its construction. This however, was not possible for the milling jar used for the batch reactions, because of the additional Teflon inlet. Therefore, this volume was determined by connecting the jar to a NOVA 3200e sorption analyzer (Quantachrome Instruments). The average volume of three consecutive measurements was 39.1 ml.

S4. Characterization methods

All samples for powder X-ray diffraction (PXRD) analysis were prepared inside a glovebox by filling 0.3 mm borosilicate glass capillaries (WJM-Glas Müller GmbH) and closing them with grease. The capillaries were subsequently flame-sealed. PXRD analyses were performed on a STOE StadiP transmission diffractometer using Mo radiation (0.7093 Å). The instrument is equipped with a primary Ge (111) monochromator (MoKα_1) and a position sensitive Mythen1K detector. Data were collected in the range between 5 and 50° (2θ) with a step width of 0.015° (2θ). The crystalline phases in the samples were identified using the PDF-2 2013 database and the ICSD database. The following files were used for the assignment (for the PDF database the PDF number is given, for the ICSD database the ICSD collection code is given): ICSD-76632 for Co (cubic), ICSD-52935 for Co (hexagonal), PDF-00-018-0325 for Cs, ICSD-421172 for $CsFeO_2$, ICSD-53236 for CsH, ICSD-15274 for CsOH, ICSD-280909 for $CsOH{\cdot}H_2O$, PDF-06-0696 for Fe, ICSD-421185 for $KFeO_2$, ICSD-43432 for KH, ICSD-47114 for $KOH{\cdot}H_2O$, ICSD-257372 for Li_2O, ICSD-51208 for $LiFeO_2$, ICSD-84971 for $LiFe_5O_8$, ICSD-44932 for Mn, ICSD-56073 for NaH, ICSD-52265 for Ni, ICSD-56084 for RbH, PDF-06-0663 for Ru.

X-ray photoelectron spectroscopy (XPS) was performed with a custom spectrometer from SPECS GmbH equipped with a Phoibos 150 1D-DLD hemispherical energy analyzer. The monochromatized Al Kα X-ray source (E = 1486.6 eV) was operated at 15 kV and 200 W. For high-resolution scans, the pass energy was set to 20 eV and for survey scans to 50 eV. The medium area mode was used as lens mode. The base pressure in the analysis chamber was 5×10^{-10} mbar during the experiment. If not given otherwise, spectra were referred to C 1s at 284.5 eV to account for charging effects. The samples were prepared inside a glovebox and transferred to the spectrometer using a gas tight transport system.

Elemental analysis was performed by Mikroanalytisches Laboratorium Kolbe (Fraunhofer Institut UMSICHT, Osterfelderstraße 3, D-46047 Oberhausen).

For the batch reactions, (IR) spectra of the product gas phase were collected in transmission mode on a Nicolet Magna IR 560 spectrometer equipped with a mercury-cadmium-telluride (MCT) detector cooled with liquid nitrogen. The gas was measured by pushing it out of the gas-sampling bag into a transmission gas cell (path length 7.5 cm) equipped with KBr windows. 32 scans were measured with a resolution of 4 cm^{-1} in the 4000-650 cm^{-1} range. Prior to every measurement, the system was flushed with nitrogen for at least 30 min and a background spectrum was taken.

For the continuous flow reactions, IR spectra of the product gas stream were collected in transmission mode on a Thermo Nicolet Avatar 370 FT-IR spectrometer equipped with a DTGS-detector and a 2 m flow cell (200 ml) heated to 150 °C. For each data point 32 scans were measured with a resolution of 4 cm^{-1} in the 4000-600 cm^{-1} range.

S5. Calculation of ammonia concentration in the gas phase, molar amount, yield and rate

The concentration of ammonia in the gas phase was determined by integrating the infrared spectrum in the region of the ammonia wagging vibration centered at around 940 cm^{-1} (see fig. S13 for exemplary spectrum).

For all calculations, ideal gas behavior was assumed and the trace amounts of methane that were formed were neglected.

Batch reaction:

With c_{NH_3} being the concentration of ammonia in the gas phase and $c_{NH_3} = \frac{n_{NH_3}}{n_{H_2}+n_{N_2}+n_{NH3}+n_{Ar}}$ it follows from $3\ H_2 + N_2 \rightarrow 2\ NH_3$ that $n_{H_2} = \frac{3}{4}\ n_0 - \frac{3}{2}\ n_{NH_3}$ and $n_{N_2} = \frac{1}{4}\ n_0 - \frac{1}{2}\ n_{NH_3}$ with n_x being the molar amount of compound x and n_0 the total initial molar amount of hydrogen and nitrogen in a stoichiometric 3:1 mixture.

With this, we can write: $c_{NH_3} = \frac{n_{NH_3}}{n_0 + n_{Ar} - n_{NH_3}}$. Rewritten we obtain $n_{NH_3} = \frac{c_{NH_3} * (n_0 + n_{Ar})}{1 + c_{NH_3}}$
with $n_{Ar} = \frac{p_{Ar} * V}{R * T}$ (p_{Ar} ≈ 101300 Pa) and $n_0 = \frac{(p - p_{Ar}) * V}{R * T}$ with p being the pressure of the experiment, V being the volume of the jar after subtracting the total volume of the milling balls, R being the ideal gas constant and T being the temperature, for which a value of 293 K was taken for calculation.

For the molar amount of ammonia we therefore get: $n_{NH_3} = \frac{c_{NH_3}}{1+c_{NH_3}} * \frac{p * V}{R * T}$

For the yield $Y_{NH_3} = \frac{n_{NH_3}}{\frac{1}{2} * n_0}$ we get $Y_{NH_3} = \frac{2 * c_{NH_3} * (n_0 + n_{Ar})}{(1 + c_{NH_3}) * n_0} = \frac{2 * c_{NH_3}}{1 + c_{NH_3}} * (1 + \frac{n_{Ar}}{n_0})$

Continuous flow reaction:

The total molar amount of ammonia produced in one experiment $n_{tot.}$ was determined by integrating over the whole course of the time dependent evolution of the ammonia concentration $c(t)$ for one experiment. For this we can write:

$$n_{tot.} = \frac{p * V_{tot.}}{R * T} = \frac{p}{R * T} * \dot{V} * \int_0^t c(t)\ dt$$

Here, $V_{tot.}$ is the total volume of gaseous ammonia and $\dot{V}$ is the initial flow rate of the gases. Even though ammonia formation is a reaction proceeding under volume reduction, due to the low amounts of ammonia produced, the initial flow rate was used as an approximation. Here, p and T are the respective pressure and temperature at which the product gas leaves the jar. For this 101300 Pa and 293 K were used for calculation.
The total yield was calculated by taking the ratio of the total amount of ammonia produced and half of the total molar amount of hydrogen and nitrogen that flew through the jar.
The rate $r(t)$ for each point in time of the experiment was calculated as follows:

$$r(t) = \frac{c(t) * \dot{V} * \frac{p}{R * T}}{m_{cat.}}$$

Results and Discussion

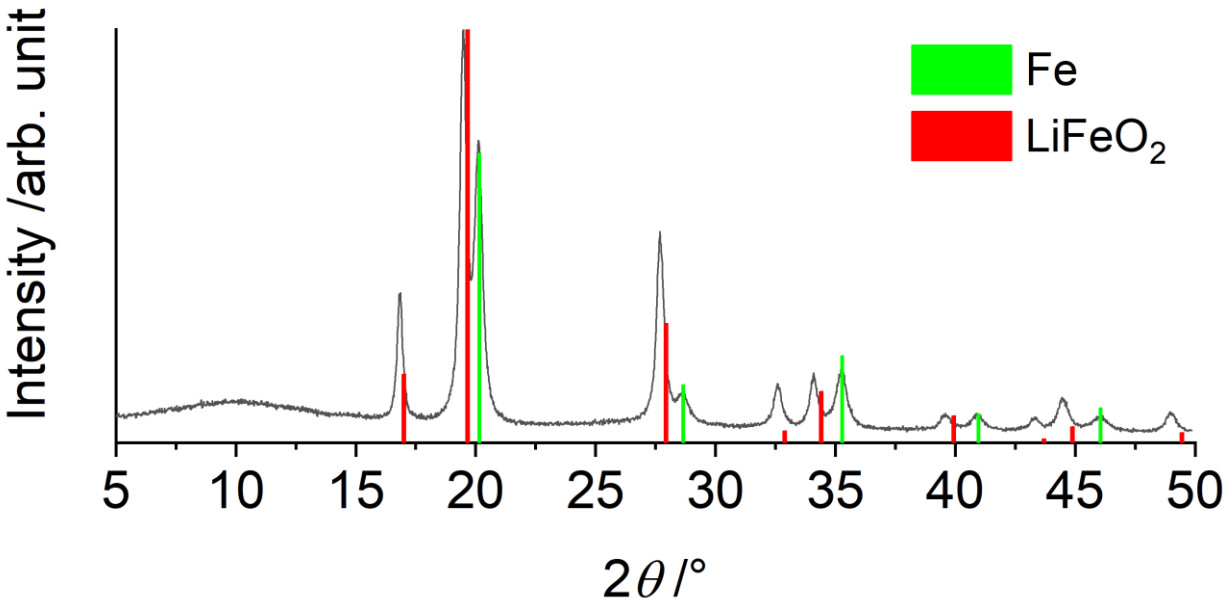

Fig. S8: PXRD of the catalyst powder after the batch reaction using $LiFeO_2$ and Fe (see table S2, entry 28). The reflections of $LiFeO_2$ were slightly shifted towards lower diffraction angles, like in all experiments when $LiFeO_2$ was ball-milled. A possible reason could be a potential reaction towards other lithium-iron-oxides with iron from the reaction or abrasion of the jar.

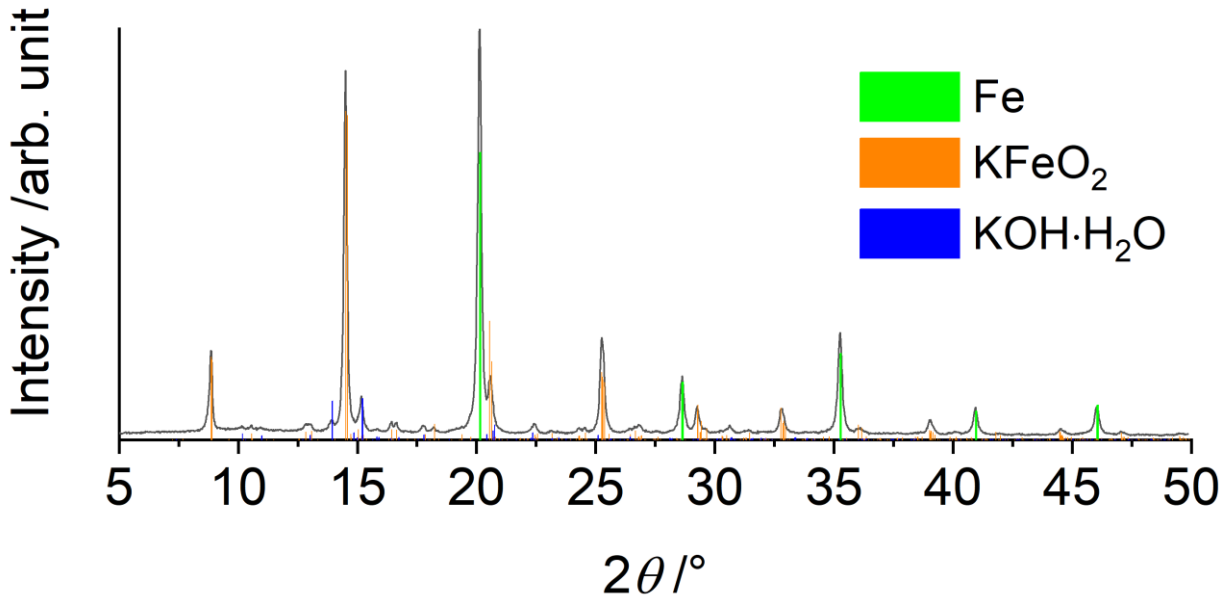

Fig. S9: PXRD of the catalyst powder after the batch reaction using $KFeO_2$ and Fe (see table S2, entry 29). Next to the reflections of the starting materials, also weak reflections of $KOH{\cdot}H_2O$ were observed, indicating an *in-situ* reduction of the $KFeO_2$ under formation of water.

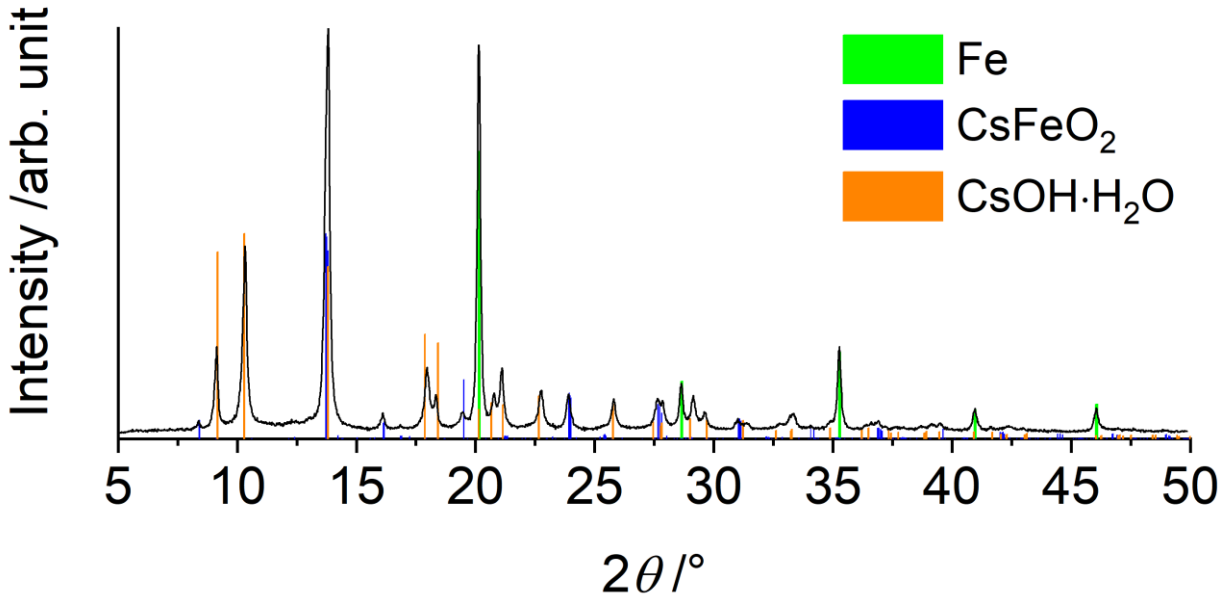

Fig. S10: PXRD of catalyst powder after the batch reaction using $CsFeO_2$ and Fe (see table S2, entry 30). Besides the reflections of the starting materials, also $CsOH \cdot H_2O$ was detected by X-ray diffraction, indicating an *in-situ* reduction of the $CsFeO_2$ under formation of water.

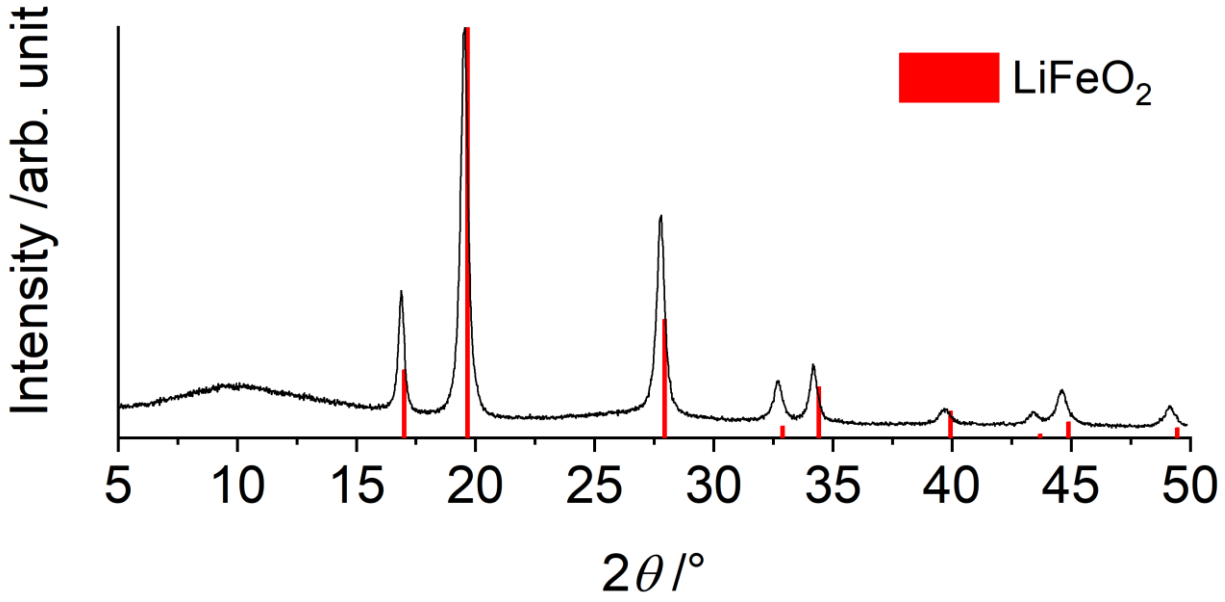

Fig. S11: PXRD of the catalyst powder after the batch reaction using pure $LiFeO_2$ (see table S2, entry 31). The reflections of $LiFeO_2$ were slightly shifted towards lower diffraction angles (see fig. S8 for comparison and explanation).

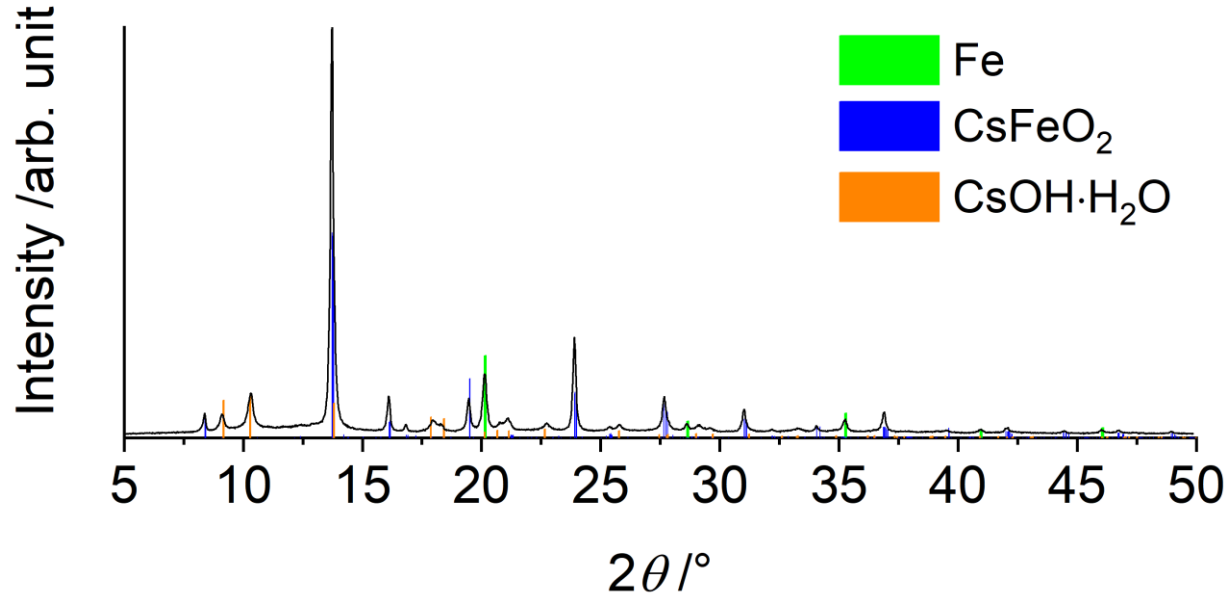

Fig. S12: PXRD of the catalyst powder after the batch reaction using pure $CsFeO_2$ (see table S2, entry 32). Besides the reflections of the starting materials, also $CsOH \cdot H_2O$ was detected by X-ray diffraction (see fig. S10 for comparison and explanation).

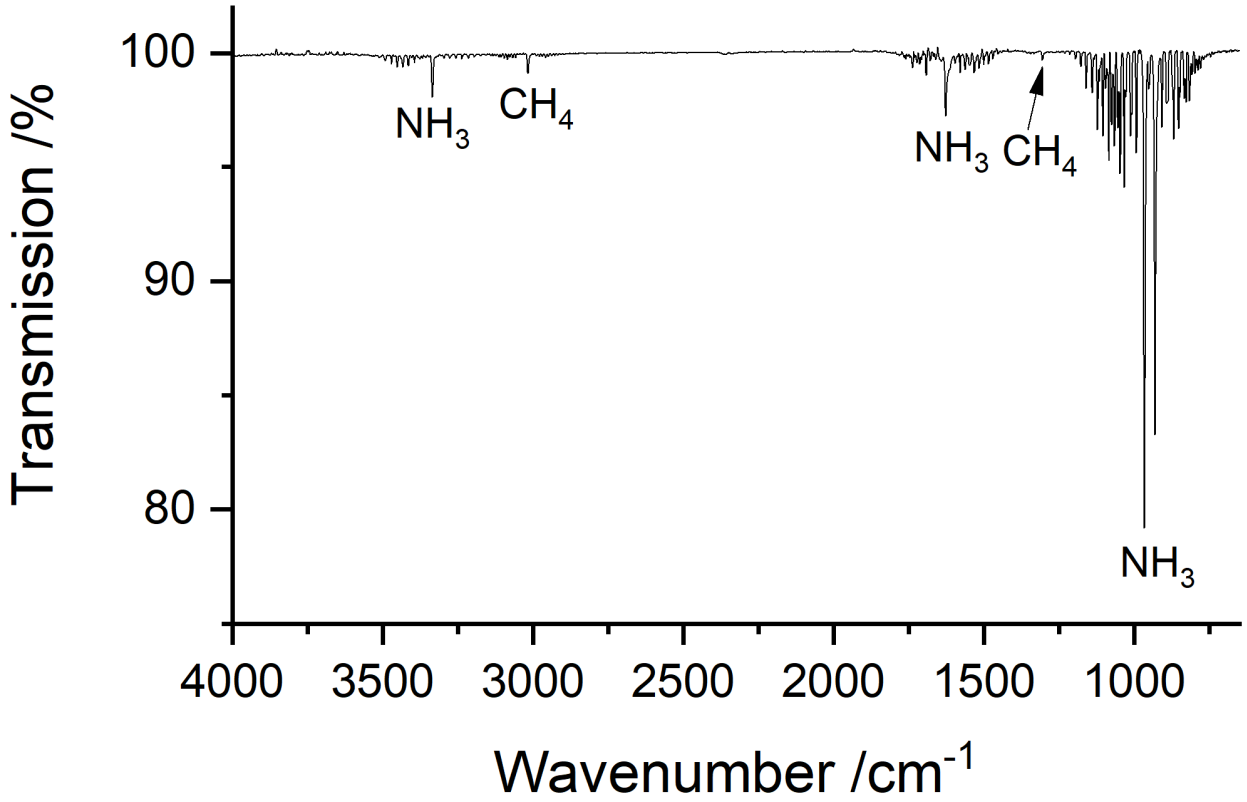

Fig. S13: Exemplary IR-spectrum of the gas phase resulting from 150 bar reaction using the FeCs catalyst (see table S2, entry 52). Besides the signals of ammonia, also methane signals can be seen, which is formed by hydrogenation of carbon-compounds in the steel or the sealings. The signals were assigned by comparison to reference spectra from the NIST standard reference database.[4]

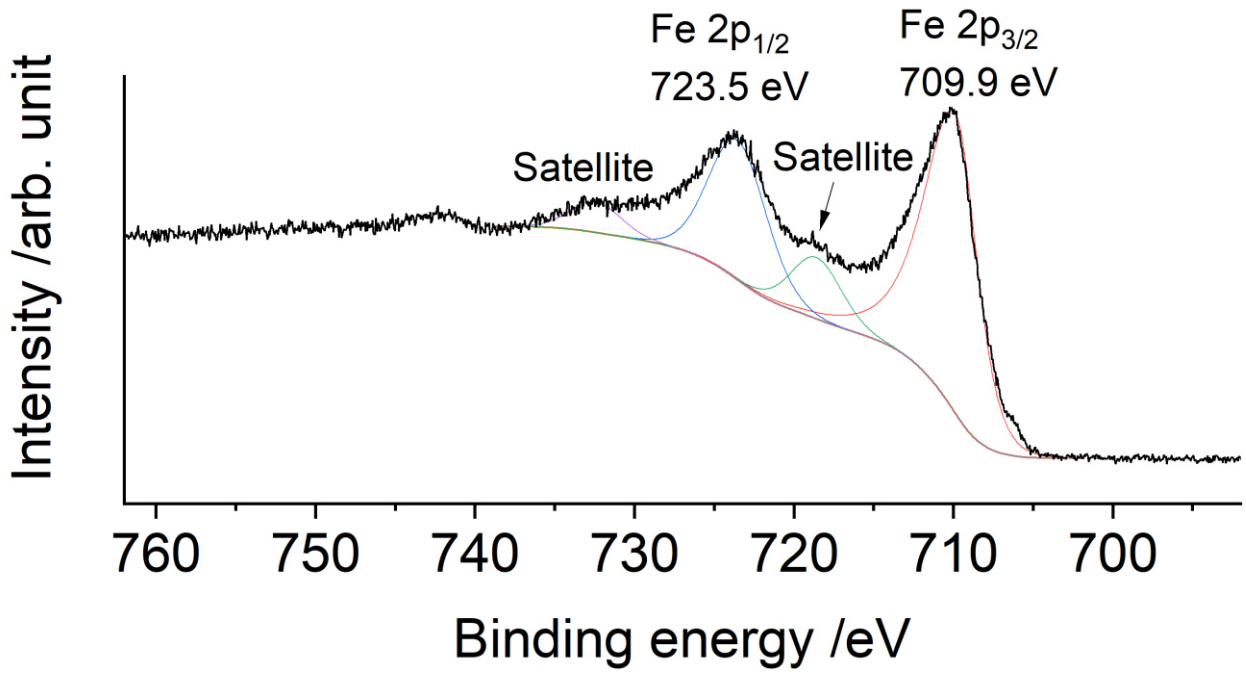

Fig. S14: XPS analysis of the iron starting material. Investigation of the Fe 2p region reveals presence of a passivated iron surface.[5] The presence of oxygen on the surface, however, is no contradiction to the statement of a catalytic and non-stoichiometric mechanochemical process for several reasons: The bulk iron is completely metallic as indicated by PXRD (see fig. S15) and elemental analysis (see table S6). For the continuous-flow experiments, no ammonia was formed in a control experiment using Li_3N (see table S5, entry 75), proving that no significant amounts of water can be formed leading to potential hydrolysis of nitride species.

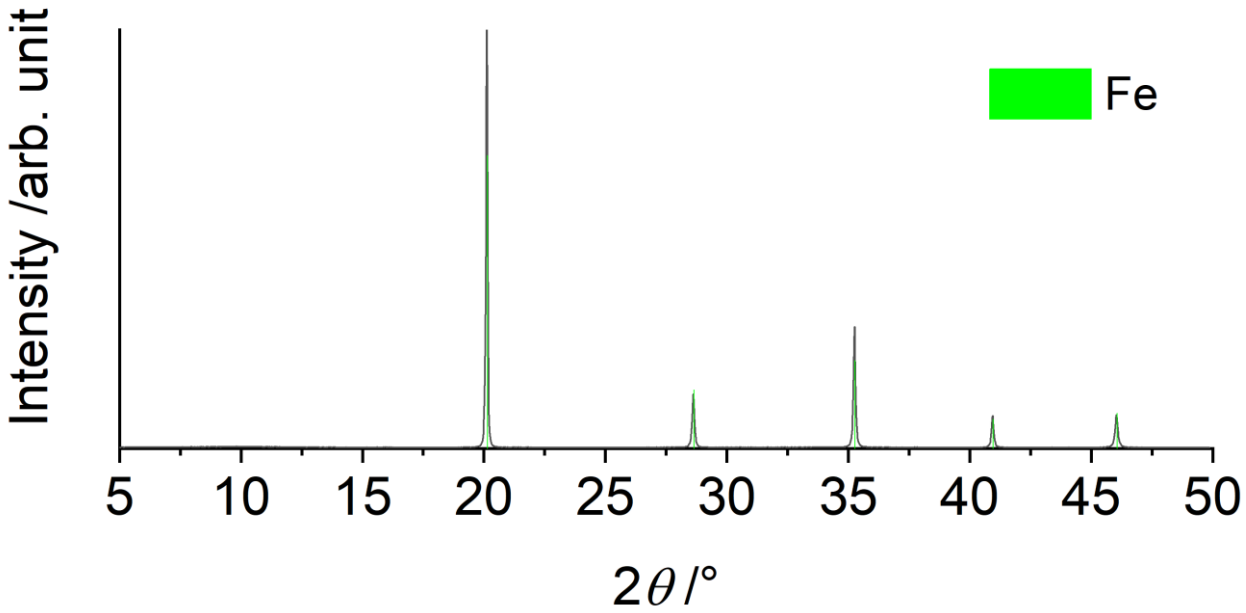

Fig. S15: PXRD of the starting iron material. No side-phases can be detected by X-ray diffraction.

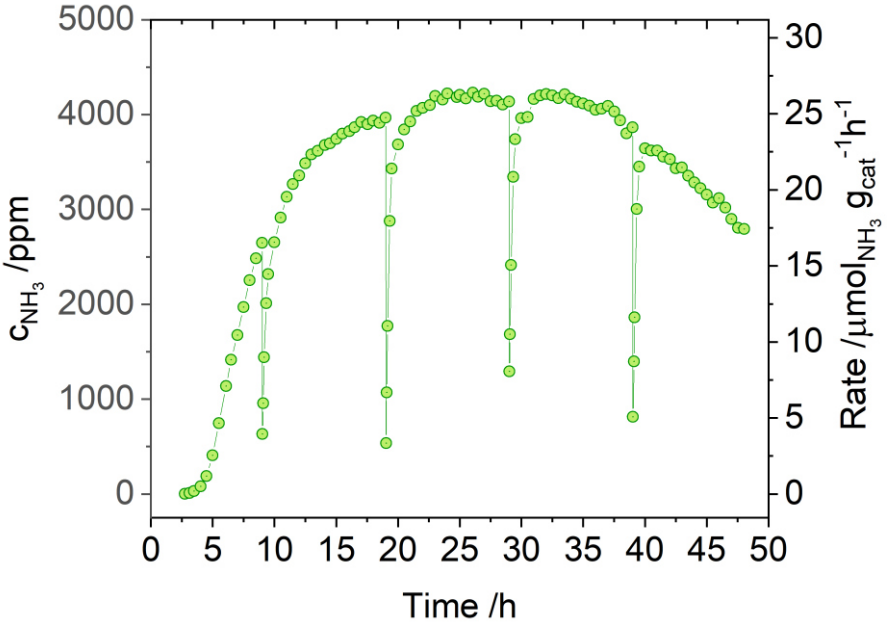

Fig. S16: Result of the continuous-flow experiment with reduced volumetric flow using 4.0 g of the FeCs catalyst. For reaction details refer to table S5, entry 72. A total gas flow of 10 ml/min instead of 20 ml/min was used in this experiment.

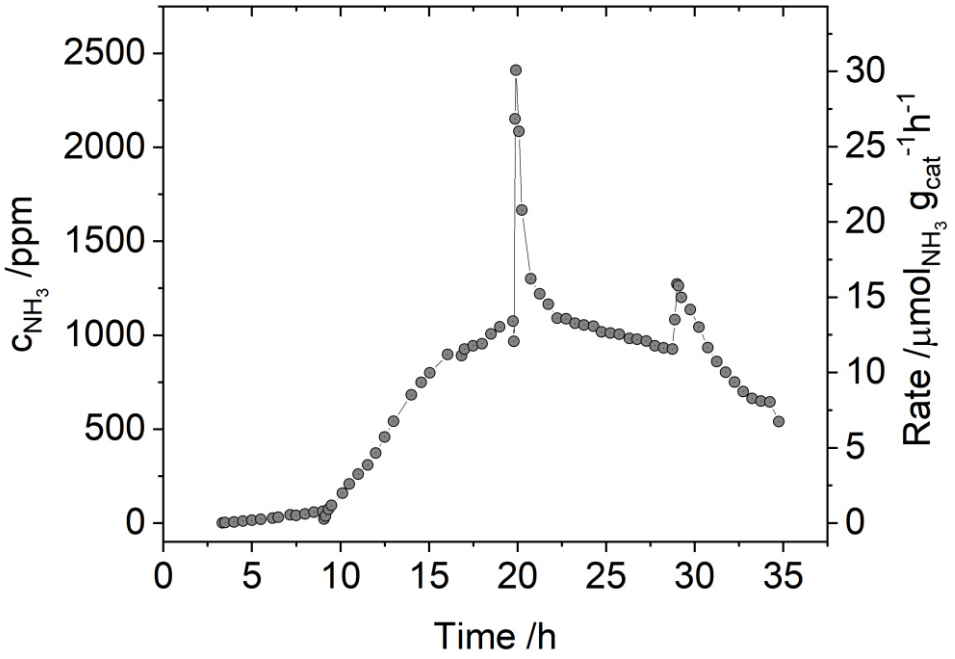

Fig. S17: Result of the continuous-flow experiment at atmospheric pressure using 4.0 g of the FeCs catalyst. For reaction details refer to table S5, entry 73. Unlike the experiments under pressure, the spikes at the restart of the milling process after pausing overnight are indicating higher ammonia concentrations. This is most likely caused by a continuing formation of ammonia in the closed jar due to the mechanochemically activated catalyst leading to higher concentrations than during the milling. Unlike the experiments that were conducted at 20 bar, no re-pressurization was necessary here and consequently no dilution occurred. Even though the additional frit was used in this experiment, a significant amount of powder was found in the funnel after the experiment. This was possibly caused by the extensive usage of the jar for several experiments before.

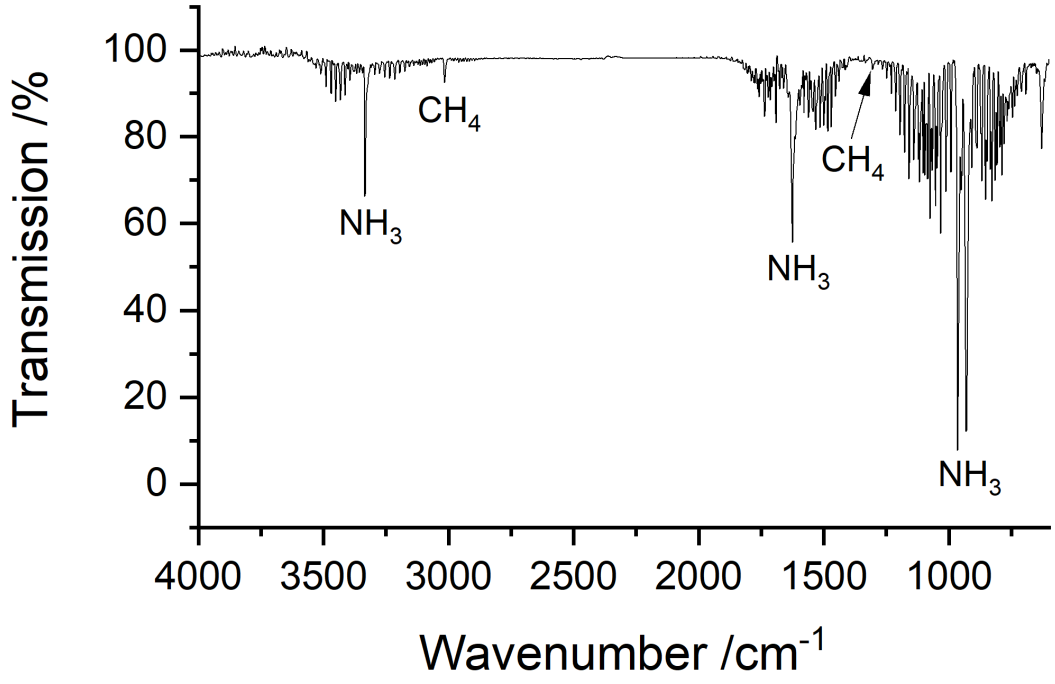

Fig. S18: Exemplary IR-spectrum of the gas phase from the continuous flow experiment using 4.0 g of the FeCs catalyst (see table S5, entry 68) after a total milling time of 18 h. Besides the signals of ammonia, also methane signals can be seen. Methane is formed by hydrogenation of carbon-compounds in the steel or the sealings. The signals were assigned by comparison to reference spectra from the NIST standard reference database.[4]

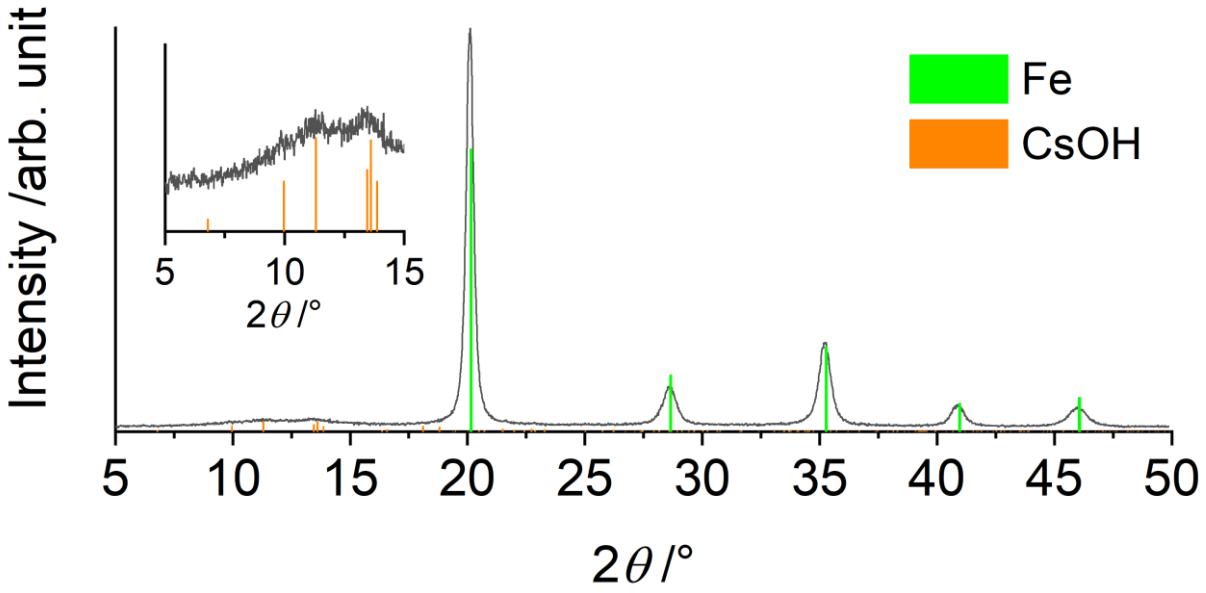

Fig. S19: PXRD of the catalyst powder after the continuous flow experiment using 4.0 g of the FeCs catalyst (see table S5, entry 68). Very weak additional reflections of CsOH are observable (see inset). The exact origin of this phase is unknown, potential reasons could be a reaction with trace amounts of water stemming from reduction of oxide species covering the surface of the milling equipment (jar, balls) or the iron used herein.

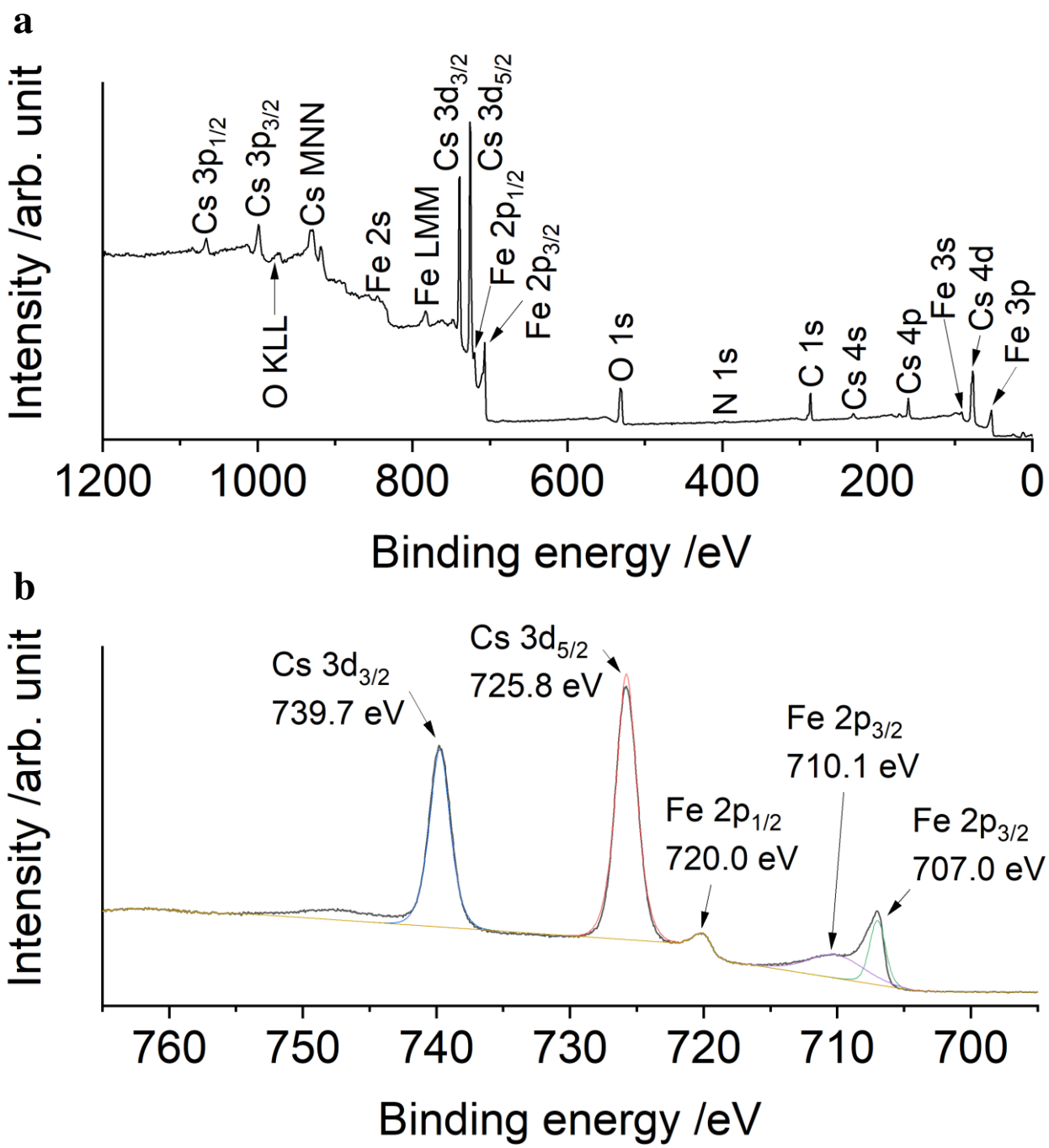

Fig. S20: XPS analysis of the catalyst powder after the continuous flow experiment using 4.0 g of the FeCs catalyst (see table S5, entry 68). The spectrum was not referenced to the C 1s signal and in order to avoid contamination of the spectrometer by potential elemental cesium, the sample was treated with a turbomolecular pump for 6h at $5 \cdot 10^{-6}$ mbar prior to the measurement. a) Survey spectrum of the sample. No significant signal of nitrogen was observed, indicating, that the nitrogen present in the sample is incorporated into the bulk material. b) Cs 3d and Fe 2p region. The positions of the Cs 3d signals are comparable to values that were obtained when cesium was coadsorbed with oxygen on metal surfaces or when Cs_2O was directly formed as a layer on a metal, indicating oxidation of the elemental cesium.[6] The Fe 2p signals are typical for partially passivated metallic iron.[5,7] This passivation layer stems from the iron starting material (see fig. S14 for XPS analysis of the iron starting material and discussion therein).

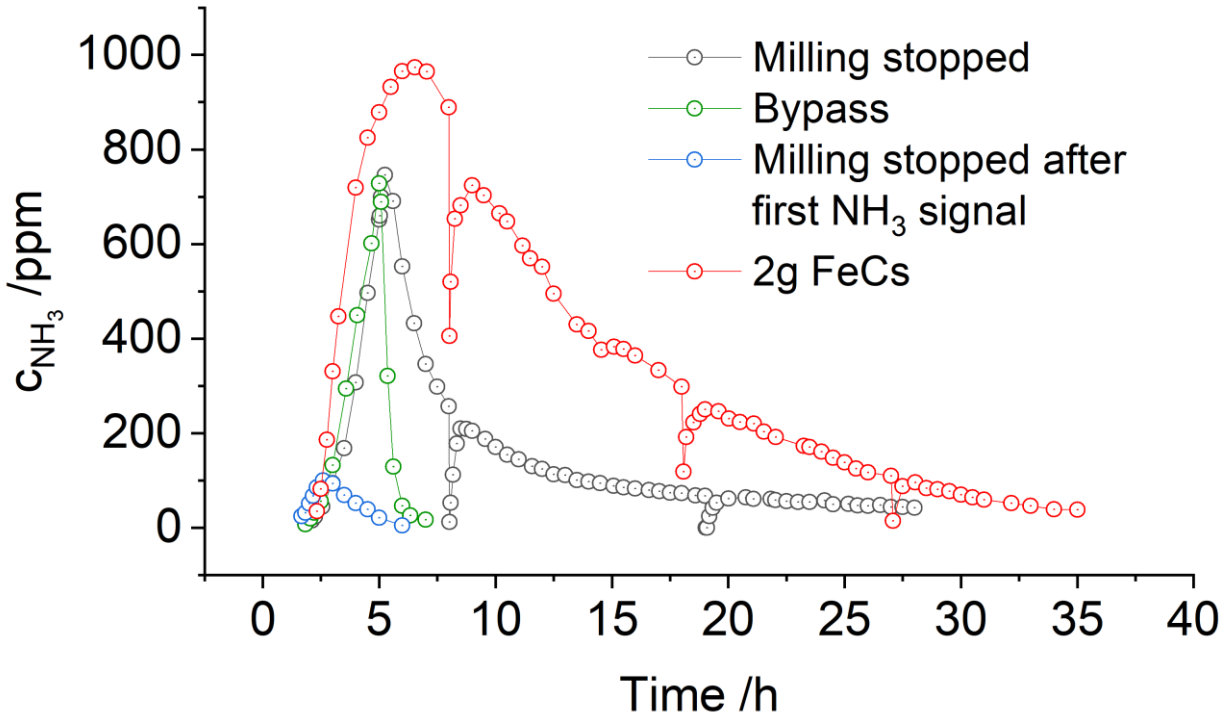

Fig. S21: Development of ammonia concentration over time for certain test experiments in the continuous-flow set-up. (red) Reference experiment with 2.0 g of the FeCs mixture (table S5, entry 65). (black) Mill was turned off after 5 h of milling (table S5, entry 71). (green) After 5 h of milling, the milling jar was bypassed (table S5, entry 70). (blue) The mill was stopped after 2 h (table S5, entry 69). For the experiment, where the milling was stopped after 5 h, the milling was continued after the ammonia concentration has reached almost 0 ppm (see fig. S22).

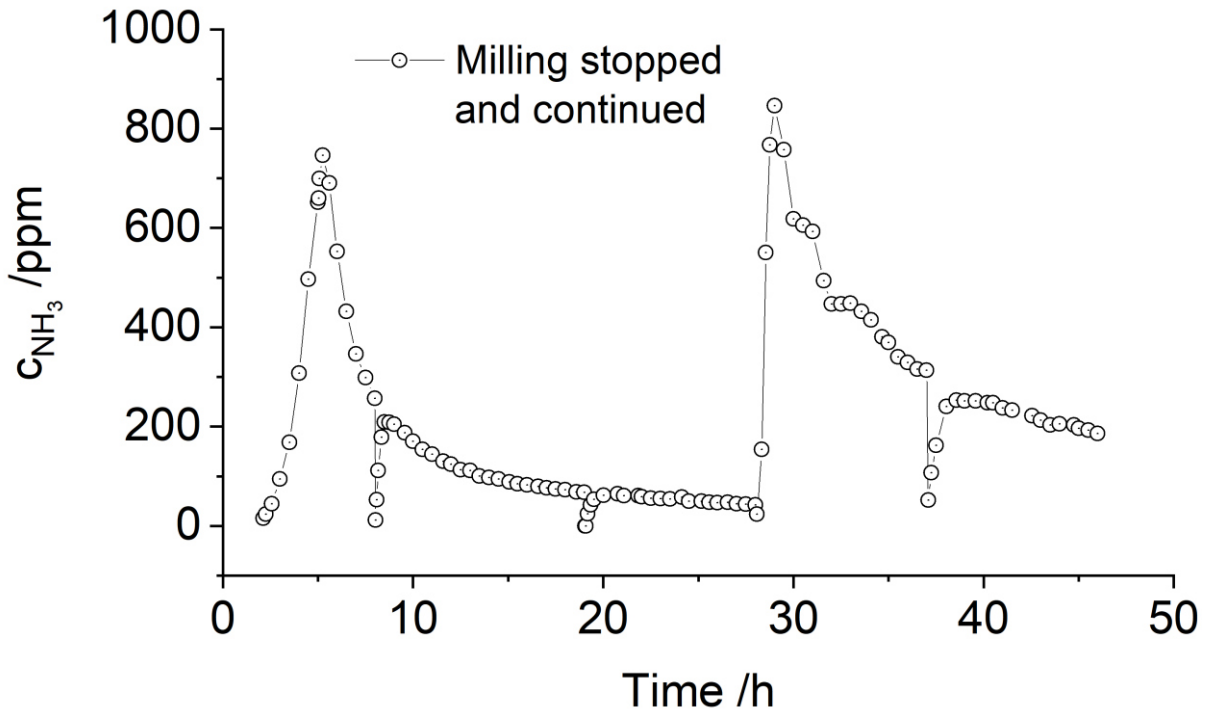

Fig. S22: Continuation of the experiment from fig. S21, where the mill was turned off after 5 h of milling. After reaching a value close to 0 ppm for the ammonia concentration, the mill was turned on again after a total time of 28 h leading again to ammonia formation.

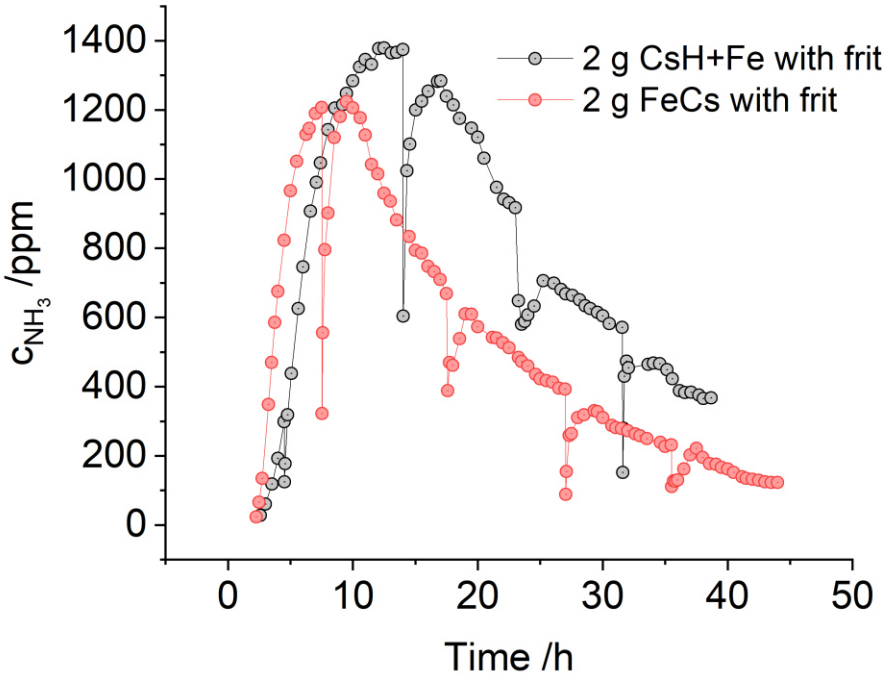

Fig. S23: Comparison of the ammonia concentration development from the continuous-flow reaction using CsH and Fe (see table S5, entry 78) and the appropriate experiment using Cs instead (table S5, entry 66). Due to the high reactivity of elemental Cs, CsH might be formed in the FeCs reactions anyway. This experiment showed, that CsH indeed leads to the formation of ammonia when combined with iron.

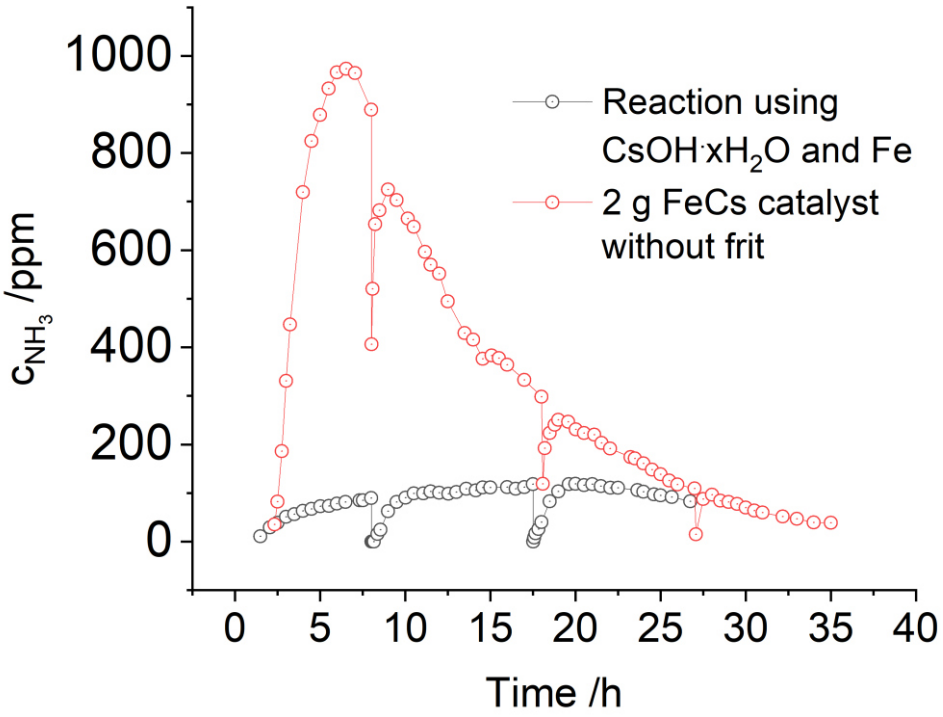

Fig. S24: Comparison of the ammonia concentration development from the continuous-flow reaction using CsOH · x H_2O and Fe (see table S5, entry 77) and the appropriate experiment using Cs instead (table S5, entry 65). Significantly lower amounts of ammonia were obtained in the reaction using CsOH · H_2O. It is assumed, that the influence of a stoichiometric reaction due to the presence of crystal water is significant here.

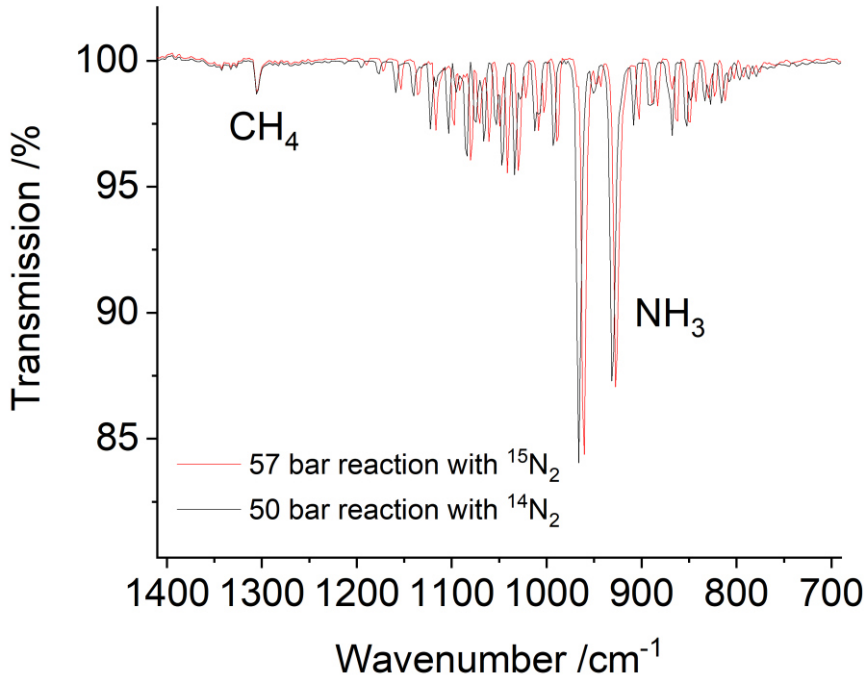

Fig. S25: Comparison of the IR spectra in the region of the ammonia wagging vibration from batch experiments using H_2 and either $^{14}N_2$ or $^{15}N_2$. See table S2, entry 42 for the conditions of the 50 bar reference experiment and table S3, entry 64 for the results of the experiment using $^{15}N_2$. A clear shift of around 4 cm^{-1} can be detected for the position of the ammonia signal when $^{15}N_2$ was used, indicating formation of $^{15}NH_3$. The value of the shift in position is in accordance with other literature data.[8]

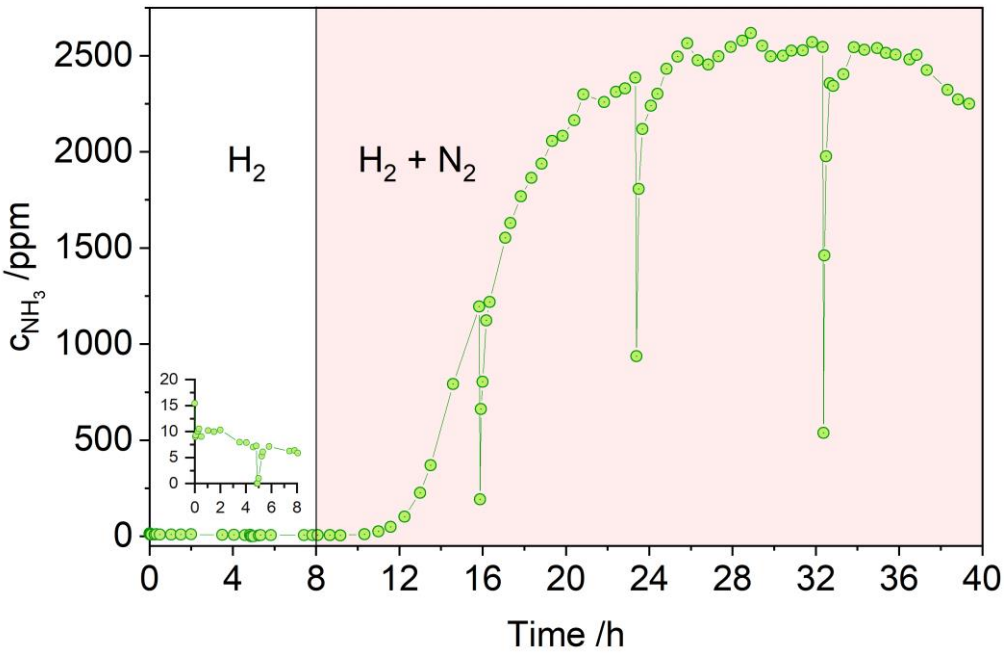

Fig. S26: Evolution of the ammonia concentration in a continuous-flow experiment using exclusively H_2 for the first eight hours (see table S5, entry 81). When no N_2 is dosed, only insignificant amounts of ammonia can be detected. These values might result from activation of nitrogen dissolved in the steel, but also traces of ammonia from previous experiments (e.g. adsorbed on the tubing) are possible. The value at 0 min with around 15 ppm corresponds to the content of ammonia in the gas phase after the first 30 min of flushing the jar (see text S2, usually the background spectrum was taken at this stage). Since no milling occurred at this point, this strengthens the hypothesis of ammonia contamination from previous experiments. In other experiments, these values of ammonia are not included in the result, because in case of the presence of traces of ammonia right from the start, they are included in the background itself. After additionally adding N_2, significant ammonia formation is observed.

Batch Reactions

Table S1: Selected batch milling experiments. For all entries, the mass of the starting materials is given, as well as the reaction pressure and the milling time. The frequency is given in revolutions per minute (rpm). For all reactions, unless noted differently, a H_2:N_2 (3:1) mixture was used as well as three steel balls of 10 mm and 15 mm diameter each. No ammonia was detected in any of the given experiments.

Entry	m_1	m_2	m_3	p /bar	t /h	f /rpm
1	Fe (0.500 g)	-	-	120	3	450
2	Fe (2.000 g)	-	-	50	24	500
3[a]	Co (0.019 g)	Mo (0.031 g)	Al_2O_3 (0.950 g)	115	3	450
4[a]	Co (0.019 g)	Mo (0.031 g)	Fe_3O_4 (0.950 g)	100	3	450
5[a]	Co (0.019 g)	Mo (0.031 g)	TiO_2 (0.950 g)	100	3	450
6[a]	Co (0.019 g)	Mo (0.031 g)	MgO (0.950 g)	100	3	450
7	Mo (1.000 g)	-	-	100	3	450
8[a]	Co (0.380 g)	Mo (0.620 g)	-	100	3	450
9	Co (1.000 g)	-	-	100	3	450
10	Ru@Al_2O_3 (0.500 g)	TiO_2 (0.500 g)	-	100	3	450
11	Ru@Al_2O_3 (0.500 g)	Fe_3O_4 (0.500 g)	-	100	3	450
12	Ru@Al_2O_3 (0.500 g)	MgO (0.500 g)	-	100	3	450
13[b]	TiN (2.000 g)	-	-	100	3	500
14[b]	Ti (2.000 g)	-	-	100	3	500
15	Al (0.200 g)	Al_2O_3 (1.800 g)	-	100	3	500
16	Ti (0.200 g)	Al_2O_3 (1.800 g)	-	100	3	500
17	Mg (0.200 g)	Al_2O_3 (1.800 g)	-	100	3	500
18	Li (0.200 g)	Al_2O_3 (1.800 g)	-	100	3	500
19	Li_3N (2.000 g)	-	-	170	6	500
20	LiH (1.000 g)	TiN (1.000 g)	-	170	6	500
21	Li (0.200 g)	TiN (1.800 g)	-	170	6	500
22[c]	LiH (1.000 g)	Fe (1.000 g)	-	170	6	500
23[c]	LiH (1.000 g)	Co (0.380 g)	Mo (0.620 g)	170	6	500
23[c]	LiH (1.000 g)	Mn (1.000 g)	-	170	6	500
24[d]	Fe (0.200 g)	CaH_2 (0.631 g)	CaF_2 (1.169 g)	50	24	500
25[d,e]	Ru (0.200 g)	CaH_2 (0.631 g)	CaF_2 (1.169 g)	50	24	500
26[d,e]	Ru (0.200 g)	BN (1.800 g)	-	50	24	500
27	Fe (0.300 g)	Ce (0.700 g)	-	50	24	500

[a]The experiments were motivated by the idea to produce a catalyst in-situ by combining Co and Mo in a 1:1 molar ratio, since this element combination has proven to result in very active ammonia synthesis catalysts.[9]

[b]The experiments were inspired by the results considering the putative TiN mechanocatalyst.[10]

[c]The experiments were motivated by the recently reported transition metal – LiH composit catalysts.[11]

[d]The experiments were motivated by the low temperature Ru/CaHF catalyst.[12]

[e]Here, a H_2:N_2 (1:1) gas mixture was used.

Table S2: Details of batch experiments with systems based on iron. For all entries, the concentration of ammonia in the gas phase, the molar amount and the yield are reported. For all reactions a H_2:N_2 (3:1) mixture was used as well as three steel balls of 10 mm and 15 mm diameter each. When no ammonia was detected in the gas phase, n.d. is given in the appropriate line. Powder X-ray diffraction patterns of the catalyst powders after milling that were not already shown in the main text are given in the following in figures S27 – S34. For entries 34 and 37, only very little ammonia was found spectroscopically, therefore no yield and no molar amount is given. For entries 39-52, two exemplary PXRDs are given for the 100 and 150 bar reaction. For the 50 bar reaction, a PXRD is given in the main text.

Entry	m_1	m_2	p /bar	t /h	f /rpm	c_{NH_3}/ppm	n_{NH_3} /mmol	Y /%
28	$LiFeO_2$ (1.500 g)	Fe (0.500 g)	50	24	500	1246	0.082	0.25
29	$KFeO_2$ (1.601 g)	Fe (0.399 g)	50	24	500	109	0.007	0.02
30	$CsFeO_2$ (1.750 g)	Fe (0.250 g)	50	24	500	19	0.001	< 0.01
31	$LiFeO_2$ (2.000 g)	-	50	24	500	n.d	n.d	n.d
32	$CsFeO_2$ (2.000 g)	-	50	24	500	n.d	n.d	n.d
33	Li (0.148 g)	Fe (1.852 g)	150	24	500	n.d	n.d	n.d
34	Li (0.100 g)	Fe (1.900 g)	50	24	50	~ 1	-	-
35	Na (0.100 g)	Fe (1.900 g)	50	24	500	36	0.002	< 0.01
36	K (0.100 g)	Fe (1.900 g)	50	24	500	149	0.010	0.03
37	K (0.030 g)	Fe (1.970 g)	50	24	500	~ 1	-	-
38	Rb (0.100 g)	Fe (1.900 g)	50	24	500	517	0.034	0.11
39	Cs (0.100 g)	Fe (1.900 g)	20	24	500	886	0.023	0.19
40	Cs (0.100 g)	Fe (1.900 g)	30	24	500	1043	0.041	0.22
41	Cs (0.100 g)	Fe (1.900 g)	40	24	500	1333	0.070	0.27
42	Cs (0.100 g)	Fe (1.900 g)	50	24	500	1447	0.095	0.29
43	Cs (0.100 g)	Fe (1.900 g)	60	24	500	1775	0.141	0.36
44	Cs (0.100 g)	Fe (1.900 g)	70	24	500	1443	0.133	0.29
45	Cs (0.100 g)	Fe (1.900 g)	80	24	500	1891	0.200	0.38
46	Cs (0.100 g)	Fe (1.900 g)	90	24	500	1518	0.180	0.31
47	Cs (0.100 g)	Fe (1.900 g)	100	24	500	1693	0.223	0.34
48	Cs (0.100 g)	Fe (1.900 g)	110	24	500	1794	0.260	0.36
49	Cs (0.100 g)	Fe (1.900 g)	120	24	500	1646	0.261	0.33
50	Cs (0.100 g)	Fe (1.900 g)	130	24	500	1819	0.312	0.37
51	Cs (0.100 g)	Fe (1.900 g)	140	24	500	1982	0.366	0.40
52	Cs (0.100 g)	Fe (1.900 g)	150	24	500	1882	0.372	0.38

Table S3: Continuation of table S2 including systems based on other transition metals. Powder x-ray diffraction patterns of the catalyst powders after milling not already shown in the main text are given in the following in figures S35– 39 (except for entry 64). For entry 53, no PXRD could be measured, because the sticky potassium adhered to the wall of the milling jar and hardly changed compared to its state when the jar was filled, just covered with a white layer (presumably KH).

Entry	m_1	m_2	p /bar	t /h	f /rpm	c_{NH_3}/ppm	n_{NH_3} /mmol	Y /%
53	Cs (1.000 g)	-	50	24	500	n.d	n.d	n.d
54	K (1.000 g)	-	50	24	500	n.d	n.d	n.d
55	Ca (0.030 g)	Fe (1.970 g)	50	24	500	n.d	n.d	n.d
56	Ba (0.103 g)	Fe (1.897 g)	50	24	500	n.d	n.d	n.d
57	Cs (0.100 g)	Mn (1.900 g)	50	24	500	n.d	n.d	n.d
58	Cs (0.100 g)	Co (1.900 g)	50	24	500	1326	0.088	0.27
59	Cs (0.100 g)	Ni (1.900 g)	50	24	500	115	0.008	0.02
60	Cs (0.100 g)	Ru (1.900 g)	50	24	500	903	0.060	0.18
61	Li_2O (1.000 g)	Fe (1.000 g)	170	24	500	100	0.022	0.02
62	Li_2O (0.294 g)	Fe (1.706 g)	170	24	500	68	0.015	0.01
63	Li_2O (0.294 g)	Fe (1.706 g)	50	24	500	n.d	n.d	n.d
64[a]	Cs (0.100 g)	Fe (1.900 g)	57	24	500	1530	0.115	0.33

[a] This experiment was performed with $^{15}N_2$. For this, the milling jar, which was loaded with catalyst and balls, was connected to the $^{15}N_2$ bottle and the connection was evacuated. Then, the milling jar was opened and also evacuated. The connection to the vacuum pump was closed and the $^{15}N_2$ bottle was opened and the gas was released into the jar. A pressure of 13.3 bar of $^{15}N_2$ was measured in the jar. The jar was then pressurized with H_2 to a final pressure of 57.0 bar (53.2 bar was targeted), giving a H_2:N_2 ratio of 3.3:1. The yield of ammonia in this case was calculated based on the amount of $^{15}N_2$.

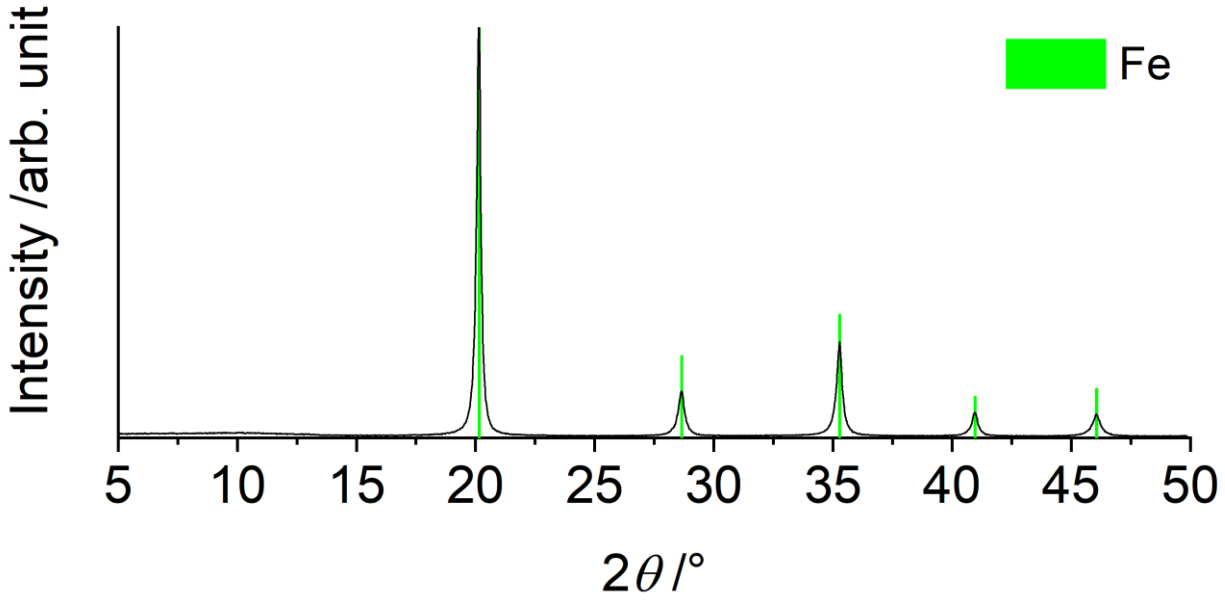

Fig. S27: PXRD of the catalyst powder after the batch reaction using Li and Fe (see table S2, entry 33). Only Fe was detected by X-ray diffraction. The concentration or crystallinity of the lithium phase(s) apparently was too low for detection.

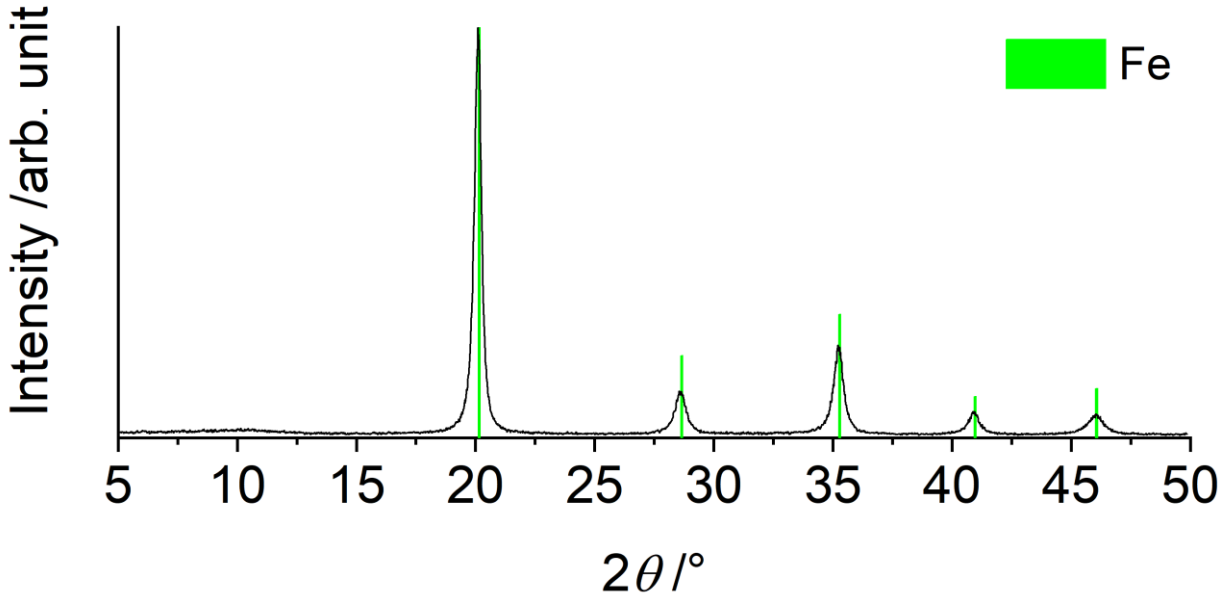

Fig. S28: PXRD of the catalyst powder after the batch reaction using Li and Fe (see table S2, entry 34). Only Fe was detected by X-ray diffraction. The concentration or crystallinity of the lithium phase(s) apparently was too low for detection.

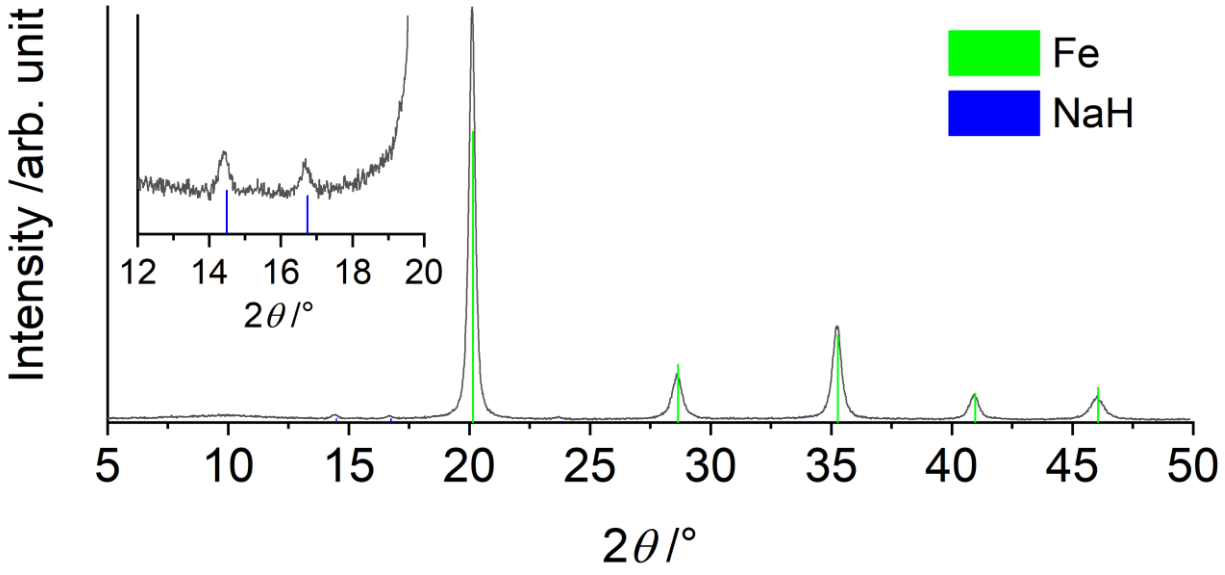

Fig. S29: PXRD of the catalyst powder after the batch reaction using Na and Fe (see table S2, entry 35). Reflections of NaH are observable, indicating the transformation of the sodium towards its hydride.

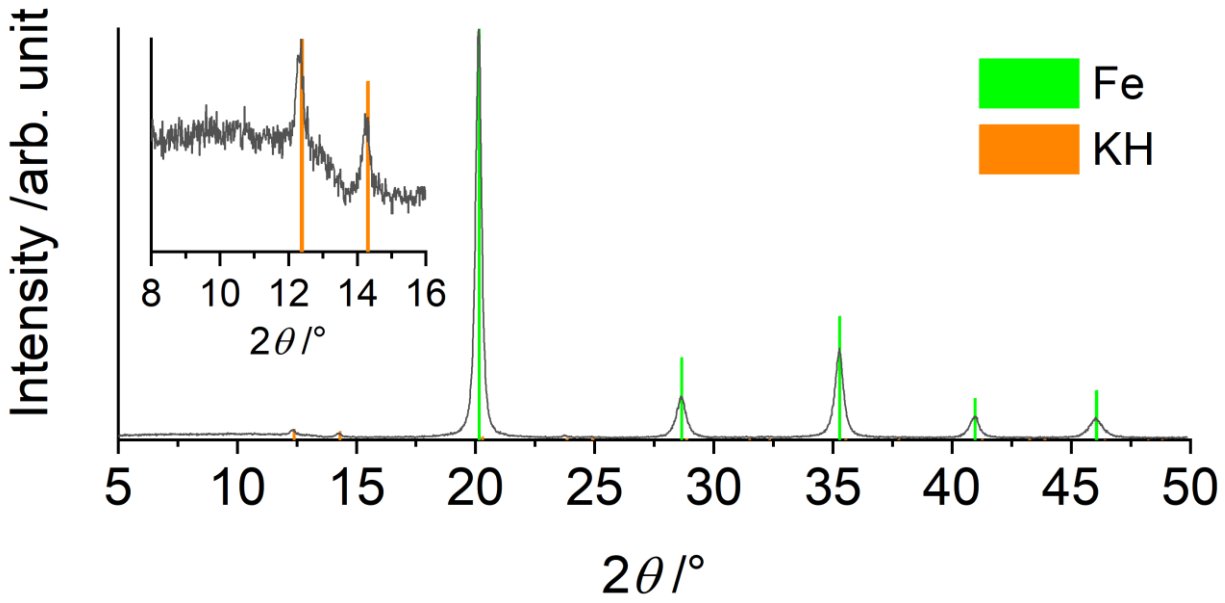

Fig. S30: PXRD of the catalyst powder after the batch reaction using K and Fe (see table S2, entry 36). Reflections of KH are observable, indicating the transformation of the potassium towards its hydride.

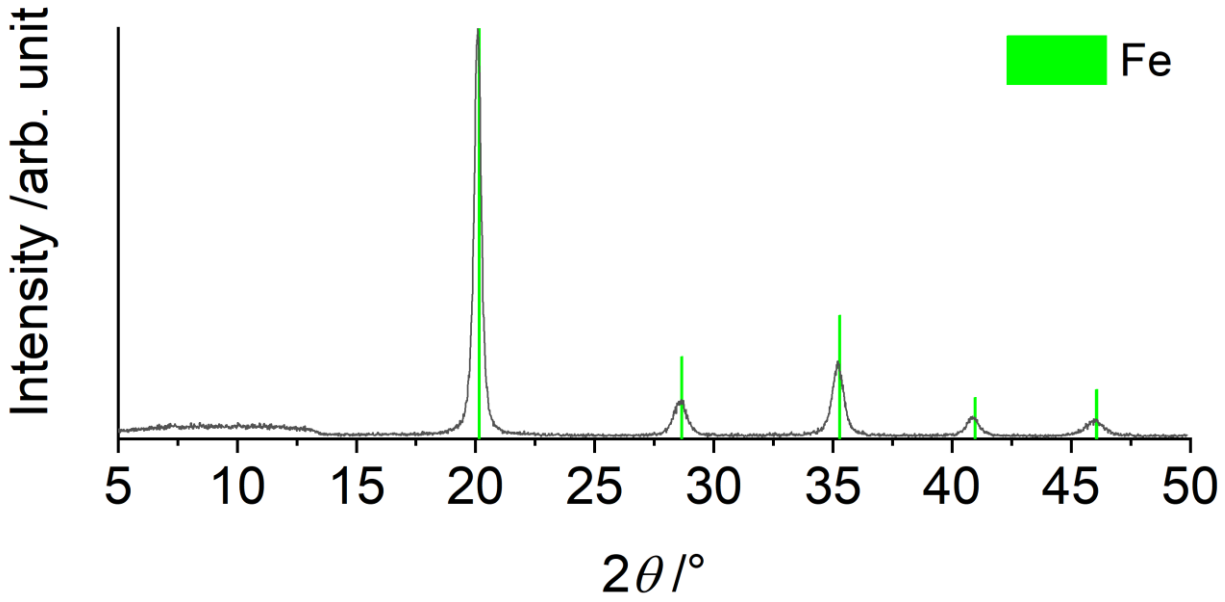

Fig. S31: PXRD of the catalyst powder after the batch reaction using K and Fe (see table S2, entry 37). Due to the lower amount of potassium used compared to entry 36, no potassium phases were detected by X-ray diffraction.

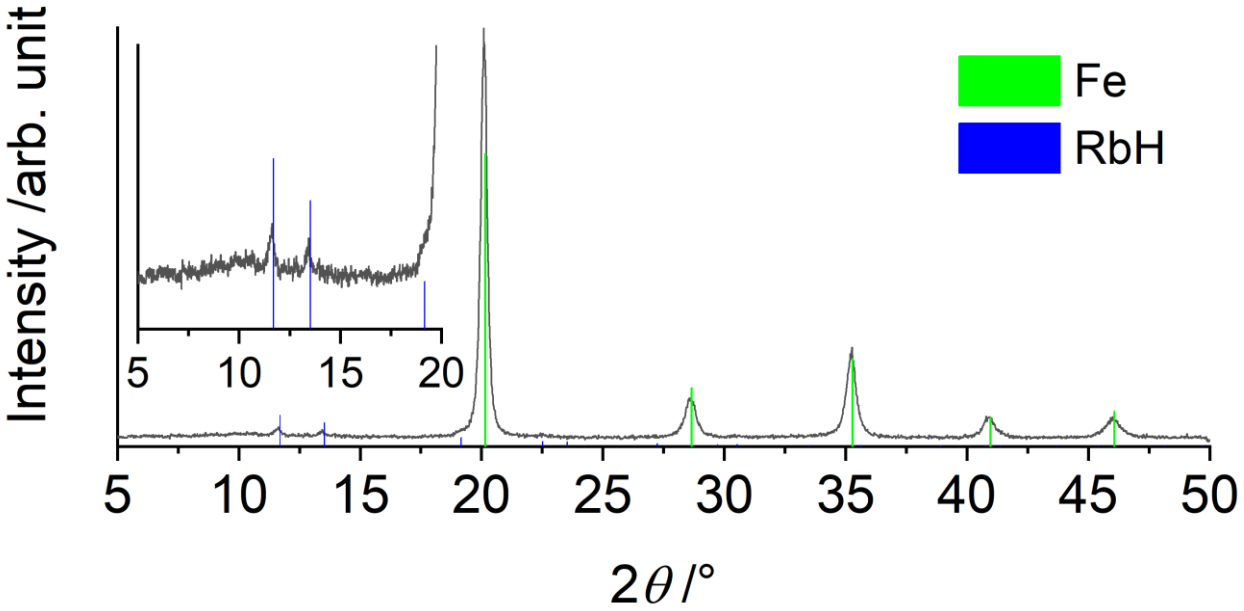

Fig. S32: PXRD of the catalyst powder after the batch reaction using Rb and Fe (see table S2, entry 38). Next to iron, also RbH was detected by X-ray diffraction, again indicating transformation of the alkali metal towards its hydride.

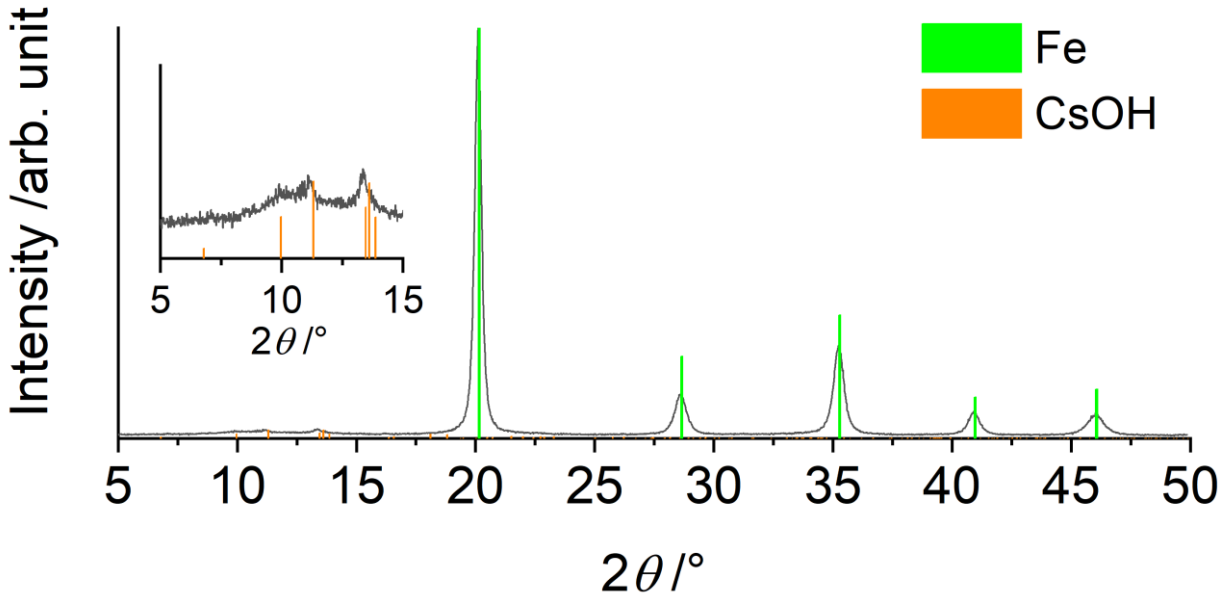

Fig. S33: PXRD of the catalyst powder after the batch reaction using Cs and Fe (100 bar reaction, see table S2, entry 47). Very weak reflections of CsOH are additionally detected by X-ray diffraction next to iron (see also fig. 1 in the main text).

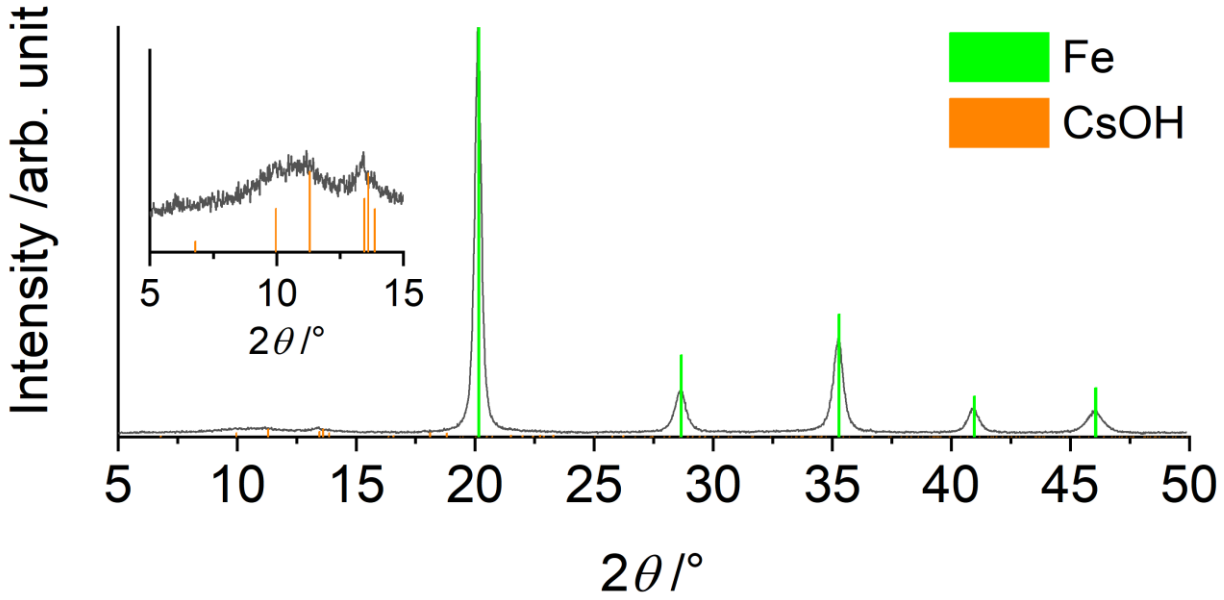

Fig. S34: PXRD of the catalyst powder after the batch reaction using Cs and Fe (150 bar reaction, see table S2, entry 52). Very weak reflections of CsOH are additionally detected by X-ray diffraction next to iron (see also fig. 1 in the main text).

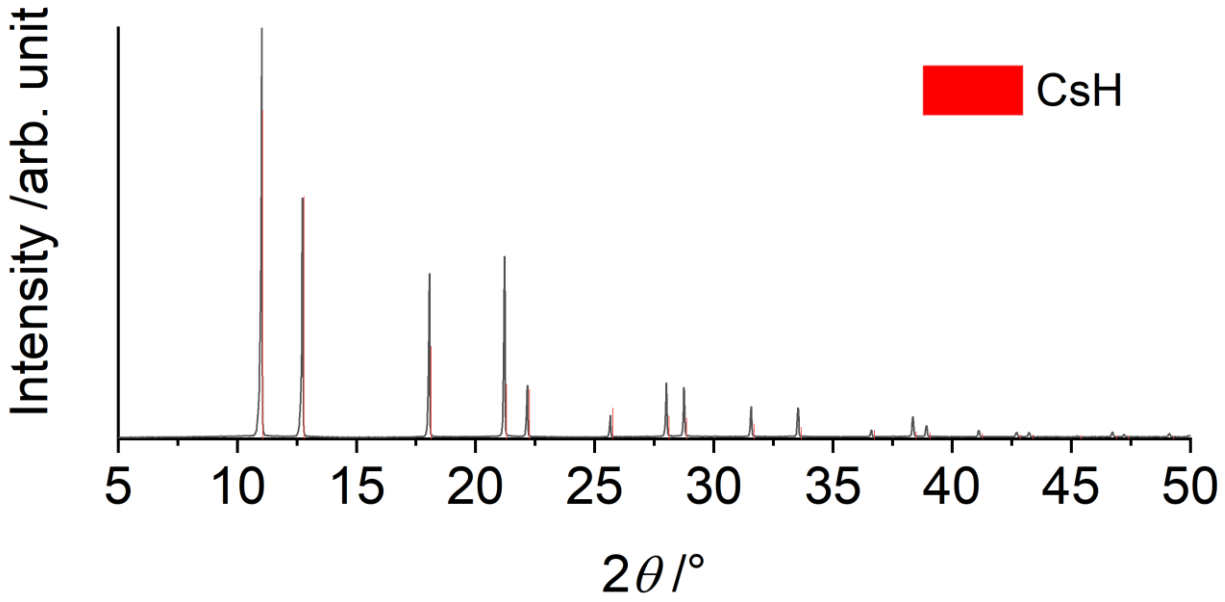

Fig. S35: PXRD of the catalyst powder after the batch reaction using only Cs. Phase pure CsH is detected by X-ray diffraction. For details refer to table S3, entry 53.

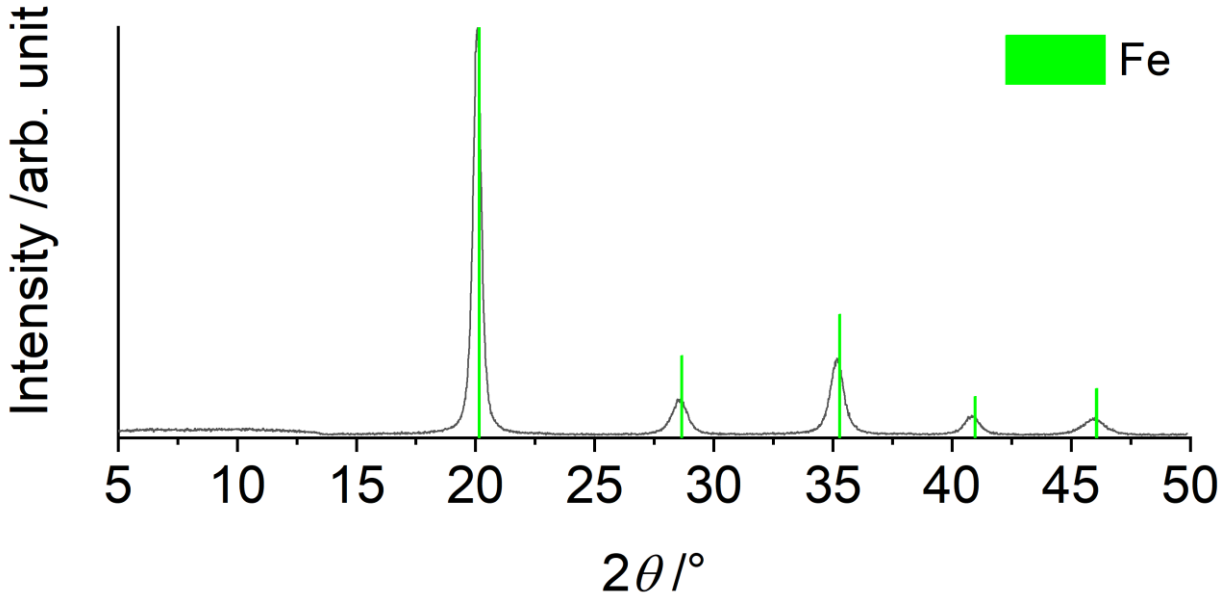

Fig. S36: PXRD of the catalyst powder after the batch reaction using Ca and Fe (see table S3, entry 55). Only Fe is detected by X-ray diffraction. The concentration or crystallinity of the calcium phase(s) apparently was too low for detection.

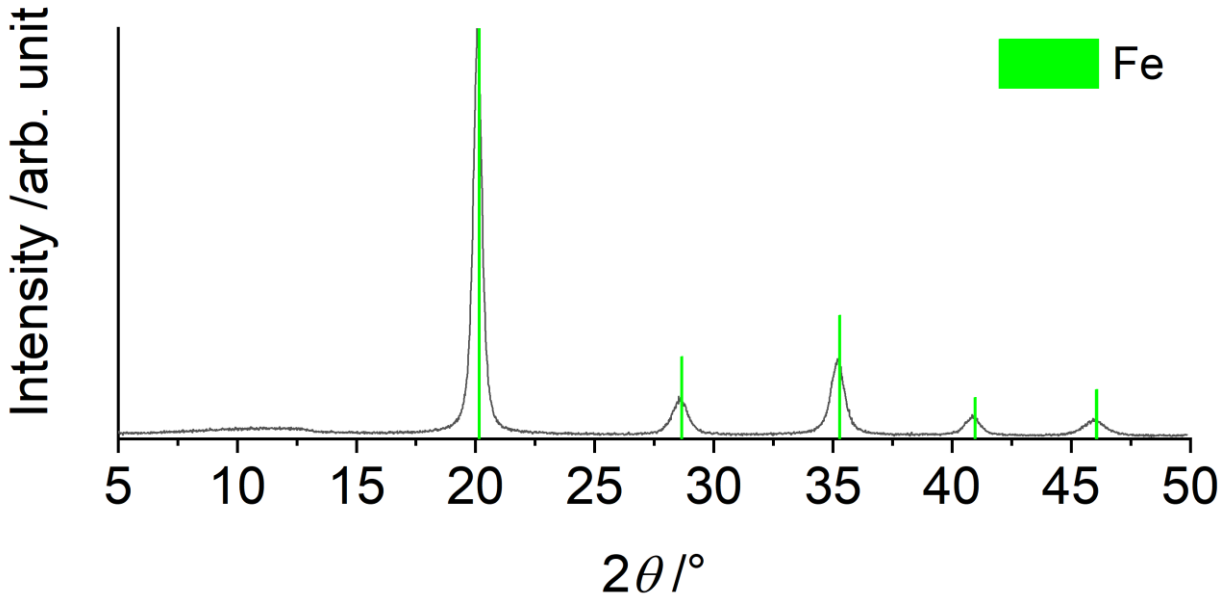

Fig. S37: PXRD of the catalyst powder after the batch reaction using Ba and Fe (see table S3, entry 56). Only Fe is detected by X-ray diffraction. The concentration or crystallinity of the barium phase(s) apparently was too low for detection.

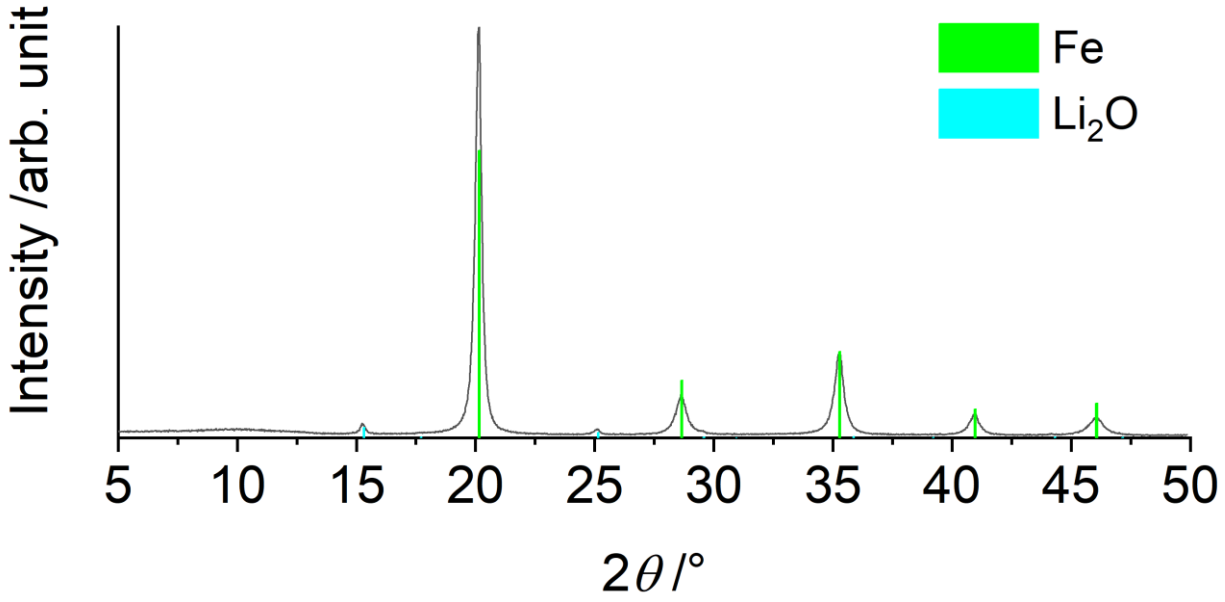

Fig. S38: PXRD of the catalyst powder after the batch reaction using Li_2O and Fe (see table S3, entry 62). Only the starting materials are detected by X-ray diffraction.

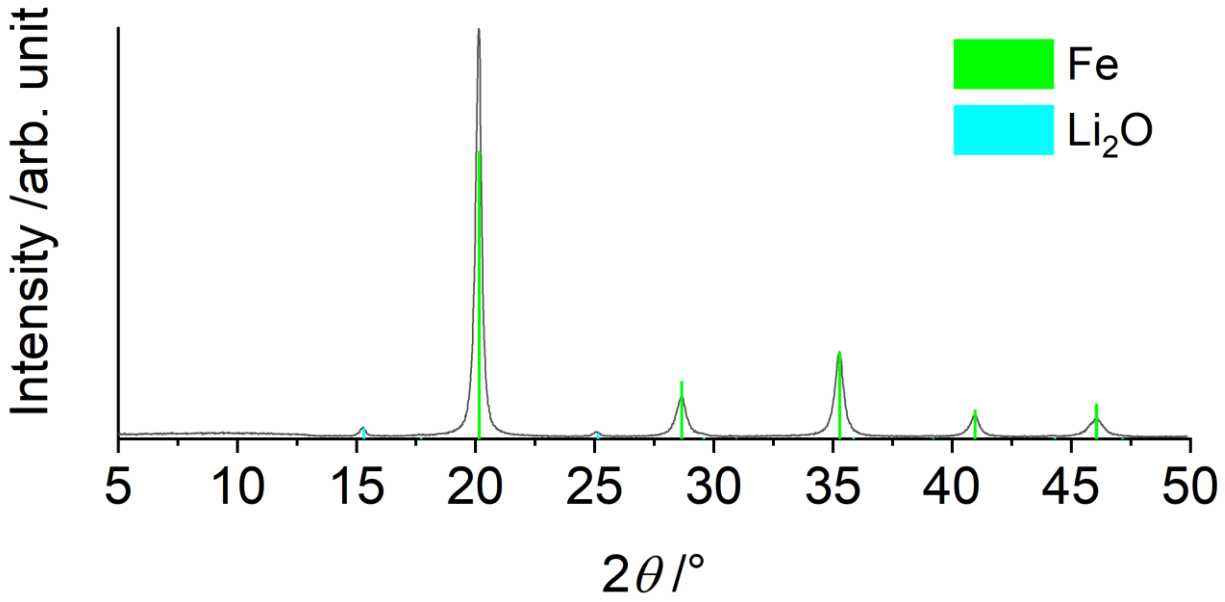

Fig. S39: PXRD of the catalyst powder after the batch reaction using Li_2O and Fe (see table S3, entry 63). Only the starting materials are detected by X-ray diffraction.

Table S4: Parameters and results of the long-term batch experiment. For all runs, the same catalyst mixture initially composed of 1,9 g of Fe and 0,1 g of Cs was used. After each run, the jar was evacuated and refilled with fresh synthesis gas. The pressure and the frequency in all runs were 50 bar and 500 rpm, respectively. Since no argon background pressure was present after the first experiment, p_{Ar} was set to 0 Pa for the calculations of the respective following experiments.

Total time /h	Time of run /h	c_{NH_3}/ppm	n_{NH_3} /mmol	Y /%
6	6	371	0.025	0.08
12	6	1127	0.074	0.23
18	6	1044	0.069	0.21
24	6	986	0.065	0.20
30	6	1110	0.073	0.22
36	6	1099	0.073	0.22
42	6	1158	0.076	0.23
48	6	638	0.042	0.13
51	3	606	0.040	0.12
54	3	594	0.039	0.12
60	6	934	0.062	0.19
63	3	648	0.043	0.13
66	3	593	0.039	0.12
72	6	928	0.061	0.19
78	6	961	0.063	0.19
81	3	547	0.036	0.11
84	3	567	0.037	0.11
132	48	3872	0.255	0.77
156	24	3145	0.207	0.63
180	24	2092	0.138	0.42
204	24	1856	0.122	0.37

Continuous-Flow Reactions

Table S5: Details of the continuous-flow experiments. For all entries, the molar amount obtained during the complete experiment and the yield of ammonia is reported. For all reactions H_2 and N_2 were mixed in a 3:1 ratio. Two steel balls of 15 mm diameter were used. All experiments were performed under a pressure of 20 bar (except for entry 71, which was conducted at atmospheric pressure). A milling frequency of 25 Hz was applied in all experiments. The total volumetric flow was 20 ml/min (STP), unless otherwise noted. When no ammonia was detected in the gas phase, n.d. is given in the appropriate line. Powder X-ray diffraction patterns (except for entry 72 and 81) not already shown at earlier stages and the full courses of ammonia concentration development (for entries 65-68) are given in the following in figures S40 – S54. The PXRD for the repetition experiment (entry 80) is not given due to no significant differences to the reference experiment (entry 67). For explanations about the additional frit, the reader is referred to fig. S6.

Entry	m_1	m_2	Additional frit?	$t_{tot.}$ /min	n_{NH_3} /mmol	Y /%
65	Cs (0.100 g)	Fe (1.900 g)	No	2100	0.566	0.06
66	Cs (0.100 g)	Fe (1.900 g)	Yes	2640	1.096	0.10
67	Cs (0.200 g)	Fe (3.800 g)	No	2970	1.927	0.16
68	Cs (0.200 g)	Fe (3.800 g)	Yes	3800	6.516	0.41
69[a]	Cs (0.100 g)	Fe (1.900 g)	No	360	0.011	< 0.01
70[b]	Cs (0.100 g)	Fe (1.900 g)	No	420	N/A	N/A
71[c]	Cs (0.100 g)	Fe (1.900 g)	No	2760	0.502	0.04
72[d]	Cs (0.200 g)	Fe (3.800 g)	Yes	2882	3.759	0.63
73[e]	Cs (0.200 g)	Fe (3.800 g)	Yes	2085	1.108	0.13
74	BN (0.100 g)	Fe (1.900 g)	Yes	420	n.d.	n.d.
75	Li_3N (0.200 g)	Fe (3.800 g)	Yes	990	n.d.	n.d.
76[f]	Li_2O (1.000 g)	Fe (1.000 g)	Yes	420	n.d.	n.d.
77[g]	$CsOH \cdot x\ H_2O$ (0.125 g)	Fe (1.875 g)	No	1605	0.111	0.02
78	CsH (0.101 g)	Fe (1.899 g)	Yes	2321	1.463	0.15
79	NaH (0.100 g)	Fe (1.900 g)	Yes	420	n.d.	n.d.
80	Cs (0.200 g)	Fe (3.800 g)	Yes	2401	3.977	0.40
81[h]	Cs (0.200 g)	Fe (3.800 g)	Yes	2362	2.793	-

[a] In this experiment, the mill was stopped after the first ammonia signal was detected (2h), in order to prove the necessity of milling impact for the continuation of ammonia formation (see fig. S21).

[b] In this experiment, the milling jar was bypassed after the ammonia concentration reached a value close to the maximum of the reference experiment (2 g of catalyst, without additional frit, entry 65), in order to examine the flush out behavior of the infrared-spectrometer (see fig. S21).

[c] In this experiment, the mill was stopped after the ammonia concentration reached a value close to the maximum of the reference experiment (2 g of catalyst, without frit, entry 65), in order to examine the development of ammonia formation without the impact of milling. After the ammonia concentration dropped to almost 0 ppm, the milling process was restarted, which again led to ammonia formation (see fig. S21 and S22).

[d] This experiment was conducted with a gas flow of 10 ml/min instead of 20 ml/min.

[e] This experiment was conducted under atmospheric pressure. Even though the additional frit was used, some powder was also pushed into the funnel in this experiment (potentially through the hole for the thermocouple after extensive usage from previous experiments).

[f] After 150 min, the total gas flow was reduced to 10 ml/min.

[g] Due to the low amount of ammonia produced in this experiment compared with the reference experiment (2.0 g of catalyst, without frit, entry 65), the production of ammonia hereby can be expected to result mostly from hydrolysis due to the present crystal water. See fig. S24 for comparison with the FeCs experiment.

[h] In this experiment, for the first eight hours, only H_2 was used with a flow rate of 20 ml/min. After that, the gas composition was changed to H_2:N_2 3:1 with a flow rate of 20 ml/min. Because of this change, no yield is given.

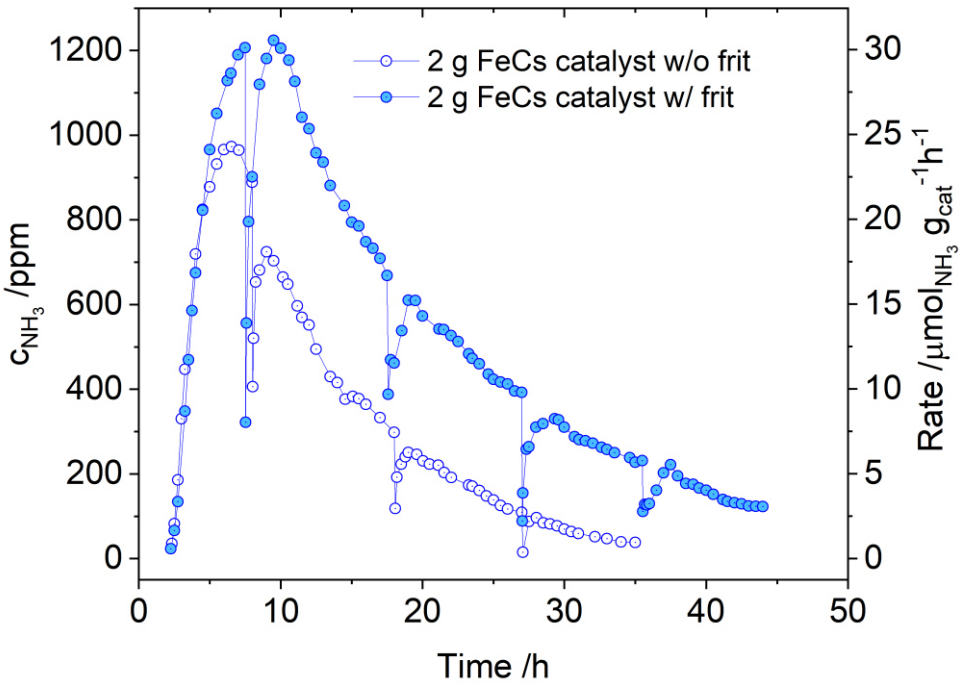

Fig. S40: Comparison of ammonia production during continuous mechanocatalysis. Comparison of experiments using 2.0 g of the catalyst, with or without the additional frit (for details refer to table S5, entries 65 and 66). Without the additional frit (see fig. S6) substantial amounts of catalyst are lost over longer milling times, leading to reduced apparent activity. The beneficial effect of the additional frit is clearly visible.

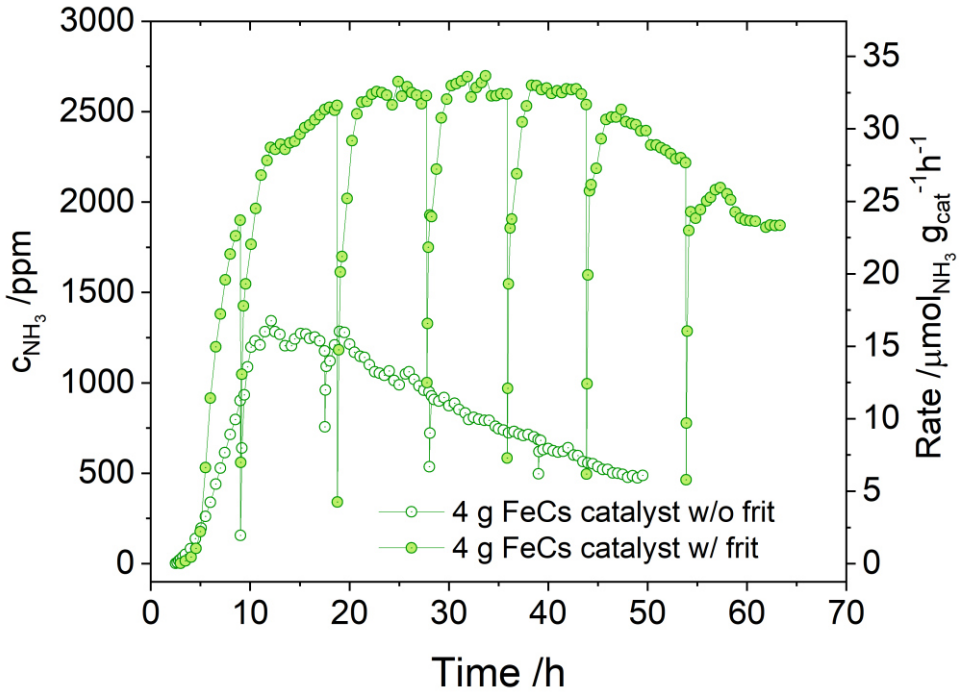

Fig. S41: Comparison of ammonia production during continuous mechanocatalysis. Comparison of experiments using 4.0 g of the catalyst, with or without the additional frit (for details refer to table S5, entries 67 and 68). Without the additional frit (see fig. S6) substantial amounts of catalyst are lost over longer milling times, leading to reduced apparent activity. The beneficial effect of the additional frit is clearly visible.

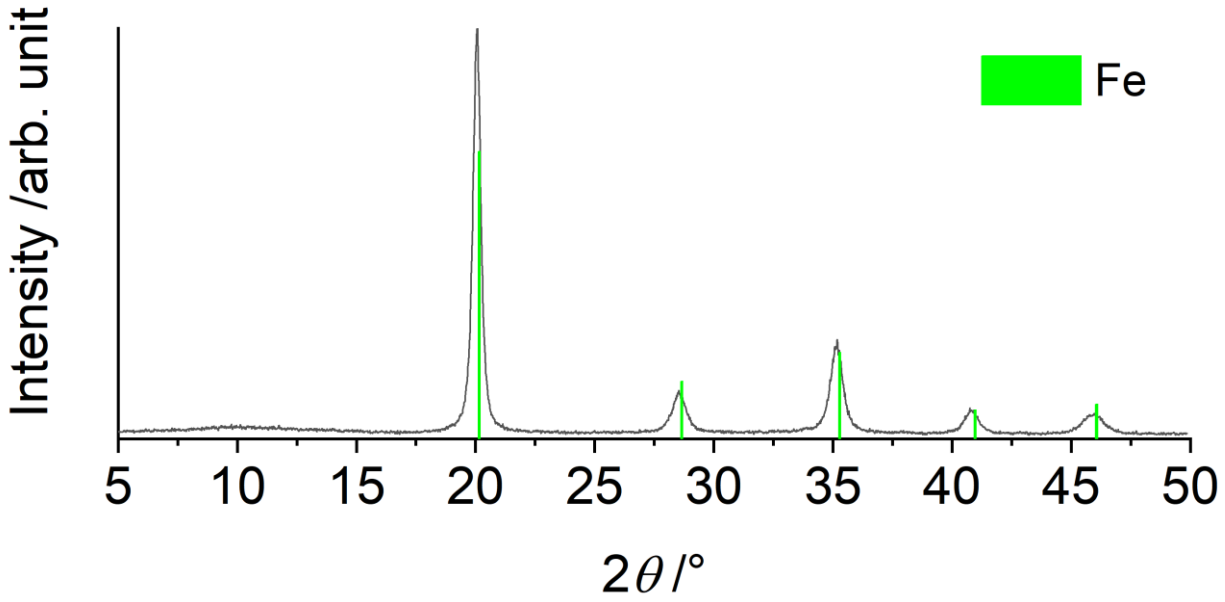

Fig. S42: PXRD of the catalyst powder after a continuous-flow reaction using Cs and Fe (see table S5, entry 65). Only Fe was detected by X-ray diffraction. The concentration or crystallinity of the cesium phase(s) apparently was too low for detection.

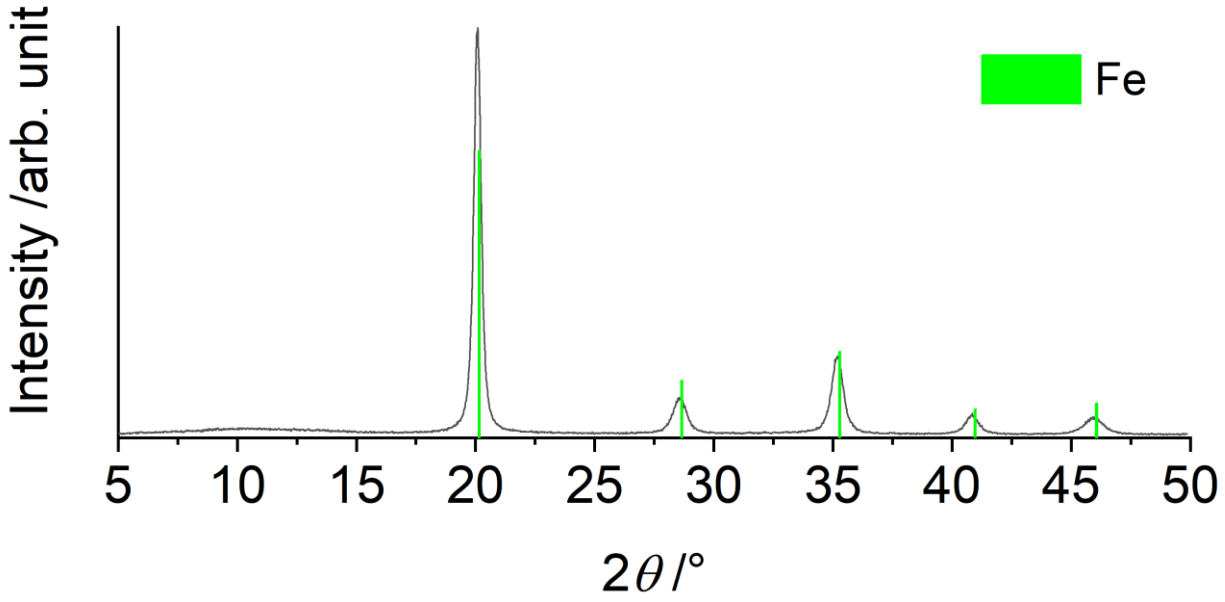

Fig. S43: PXRD of the catalyst powder after a continuous-flow reaction using Cs and Fe (see table S5, entry 66). Only Fe was detected by X-ray diffraction. The concentration or crystallinity of the cesium phase(s) apparently was too low for detection.

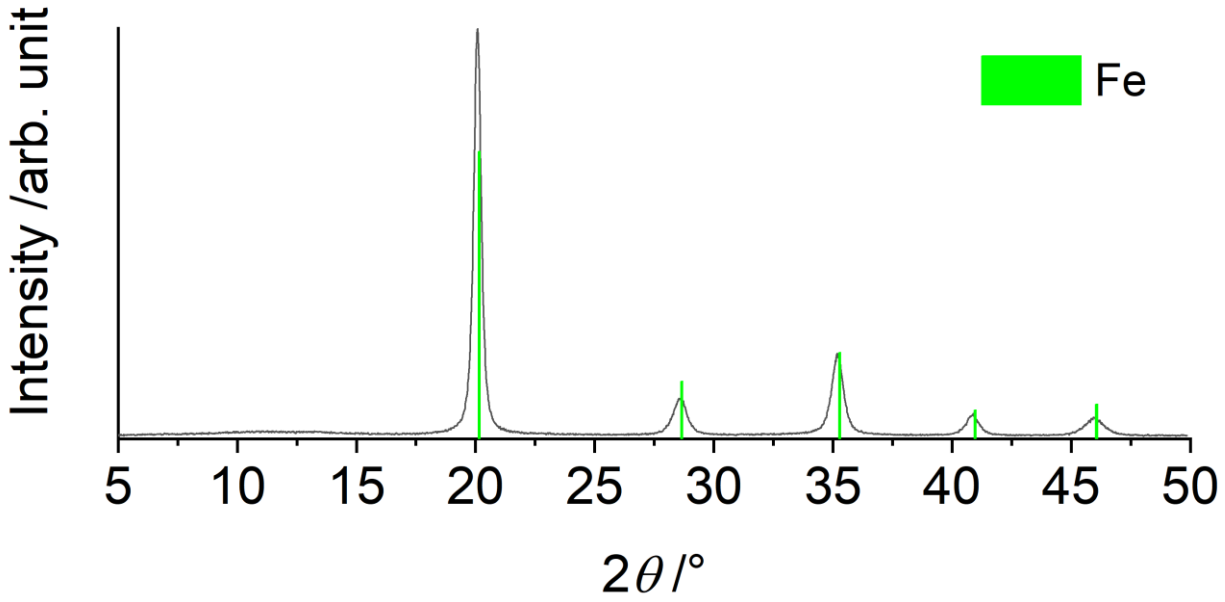

Fig. S44: PXRD of the catalyst powder after a continuous-flow reaction using Cs and Fe (see table S5, entry 67). Only Fe was detected by X-ray diffraction. The concentration or crystallinity of the cesium phase(s) apparently was too low for detection.

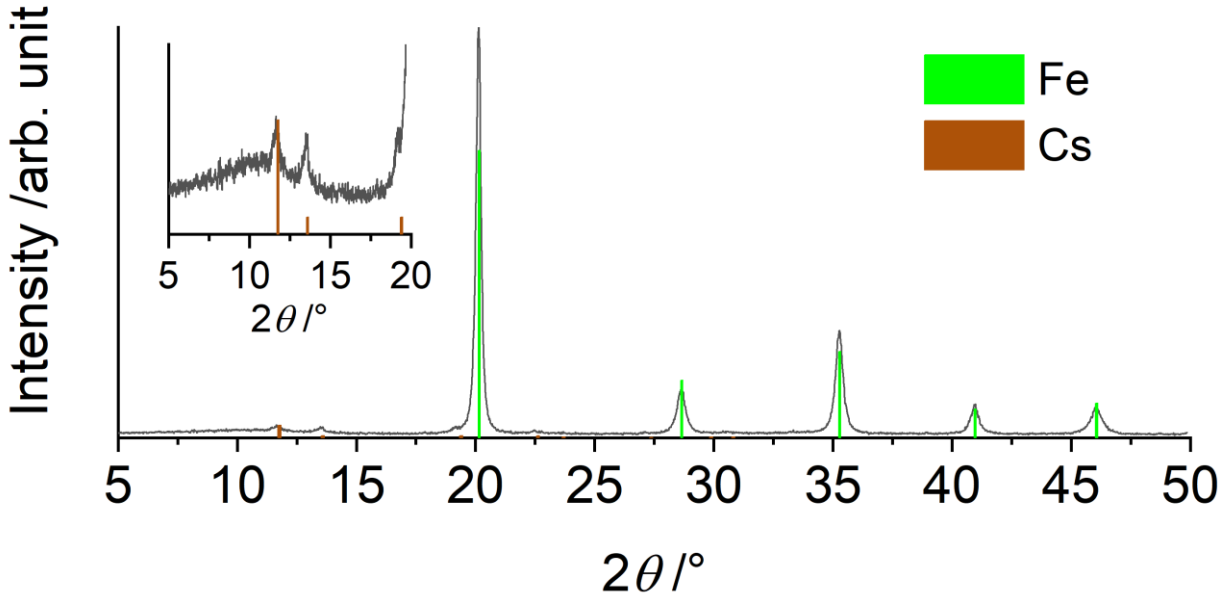

Fig. S45: PXRD of the catalyst powder after a continuous-flow reaction using Cs and Fe (see table S5, entry 69). The assignment of the additional reflections to elemental cesium is questionable, because the parameters of the database entry were much different concerning the measurement pressure. However, no other phase was found matching the additional reflections. Besides that, only Fe was detected by X-ray diffraction.

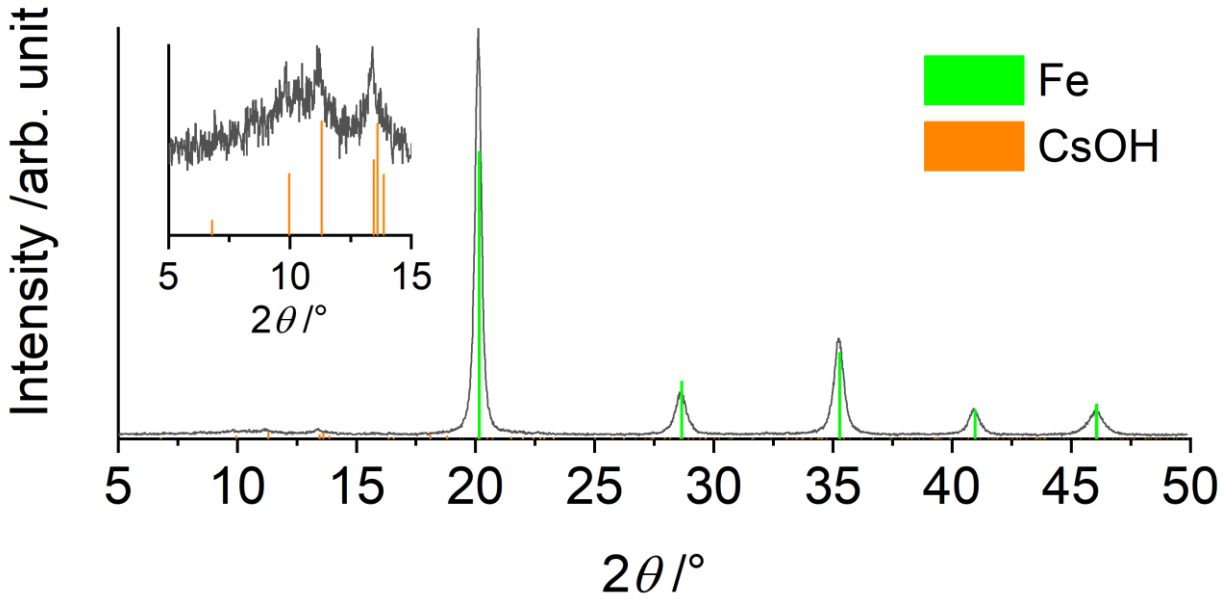

Fig. S46: PXRD of the catalyst powder after a continuous-flow reaction using Cs and Fe (see table S5, entry 70). Fe and weak reflections of CsOH are detected by X-ray diffraction. For comparison and potential causes for the presence of CsOH see fig. S19 and explanations therein.

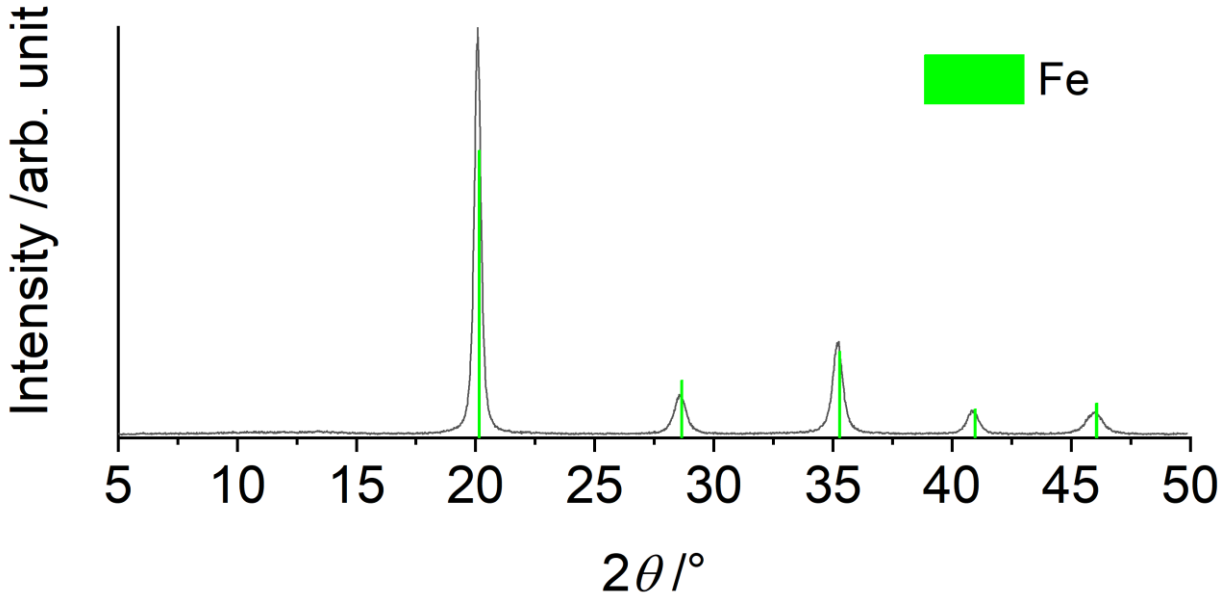

Fig. S47: PXRD of the catalyst powder after a continuous-flow reaction using Cs and Fe (see table S5, entry 71). Only Fe was detected by X-ray diffraction. The concentration or crystallinity of the cesium phase(s) apparently was too low for detection.

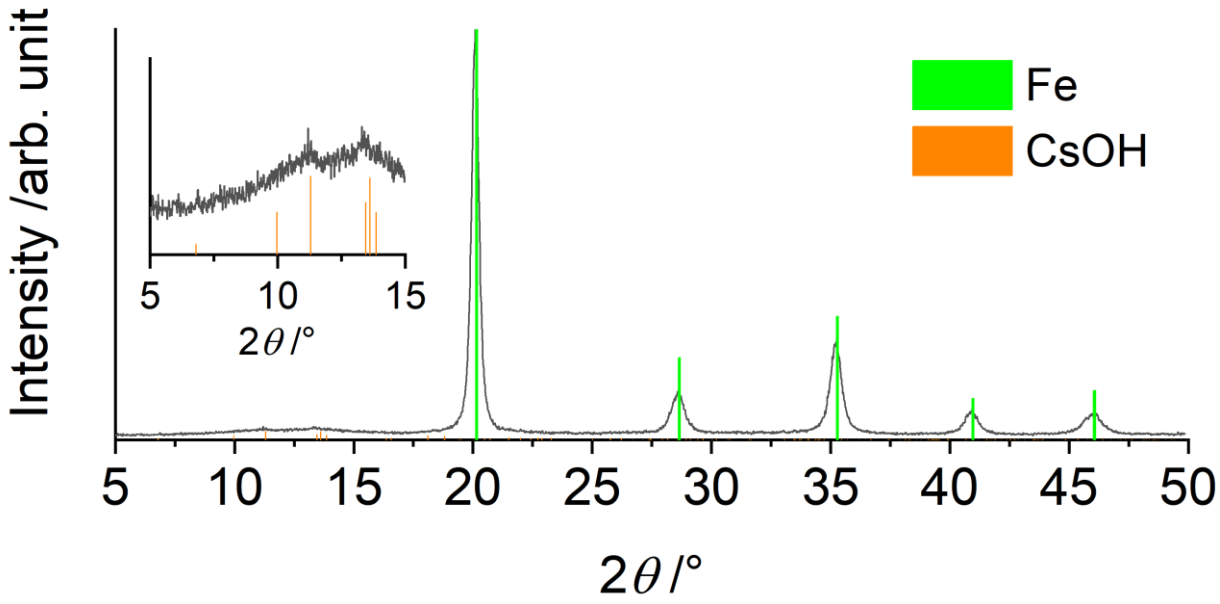

Fig. S48: PXRD of the catalyst powder after a continuous-flow reaction using Cs and Fe (see table S5, entry 73). Fe and weak reflections of CsOH are detected by X-ray diffraction. For comparison and potential causes for the presence of CsOH see fig. S19 and explanations therein.

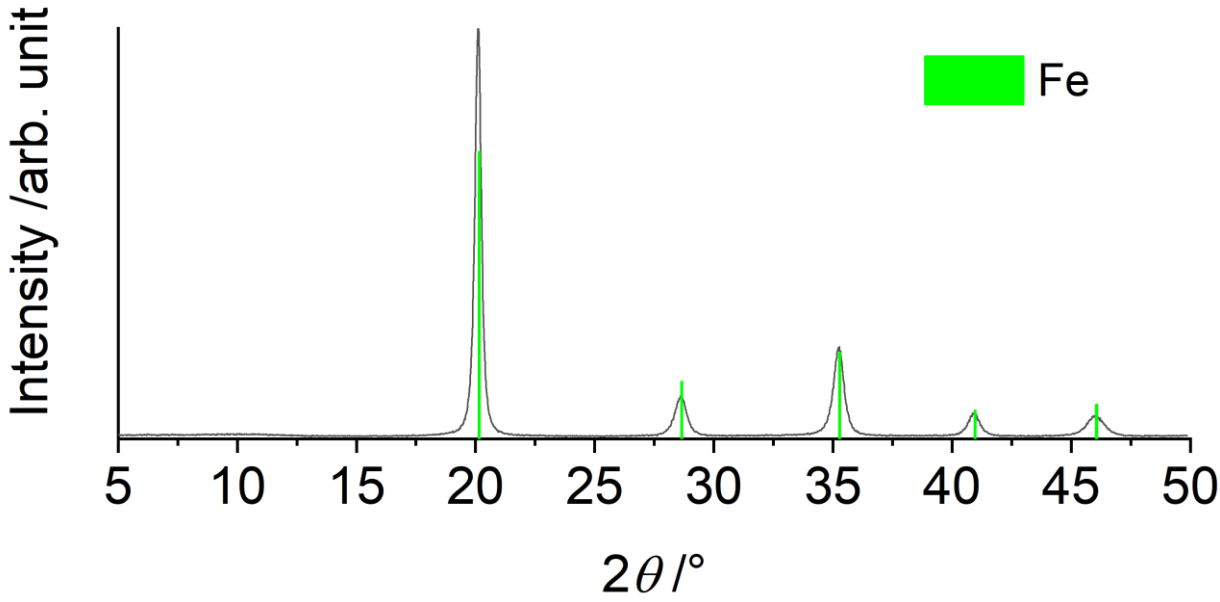

Fig. S49: PXRD of the catalyst powder after the continuous-flow reaction using BN and Fe (see table S5, entry 74). Only Fe is detected by X-ray diffraction. The concentration or crystallinity of the BN phase apparently was too low for detection.

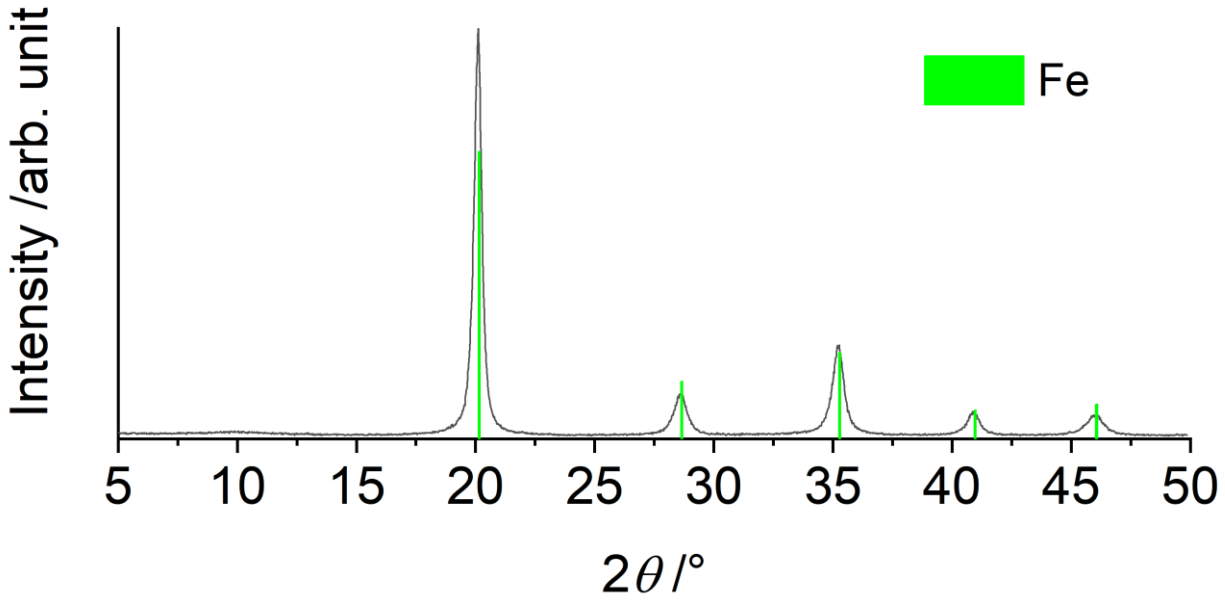

Fig. S50: PXRD of the catalyst powder after the continuous-flow reaction using Li_3N and Fe (see table S5, entry 75). Only Fe is detected by X-ray diffraction. The concentration or crystallinity of the lithium phase(s) apparently was too low for detection.

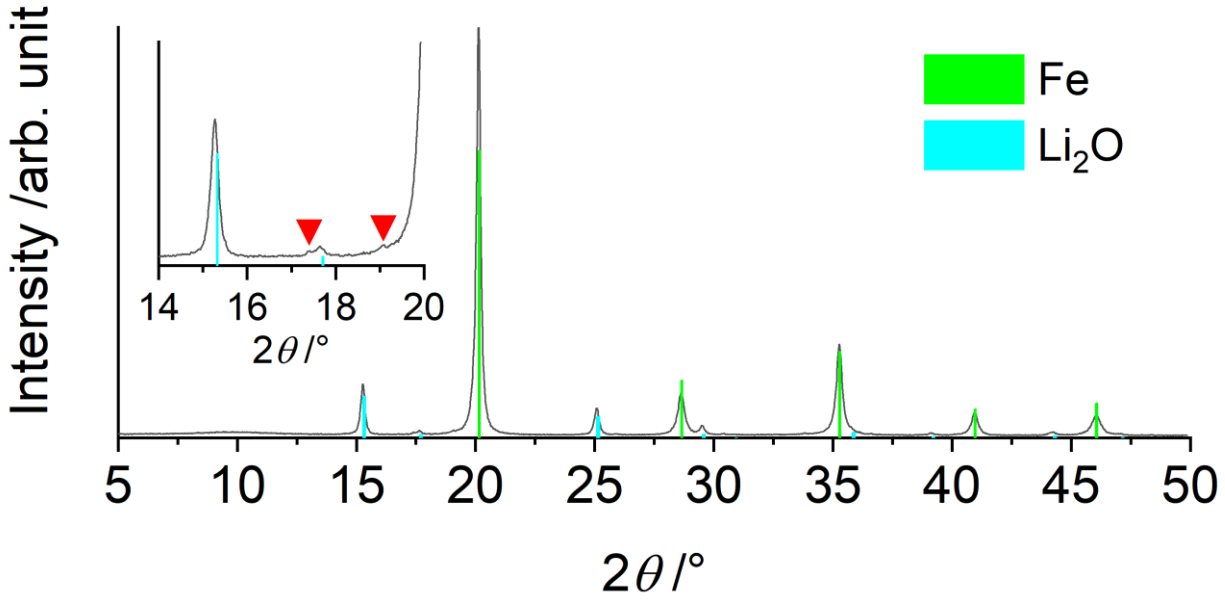

Fig. S51: PXRD of the catalyst powder after the continuous-flow reaction using Li_2O and Fe (see table S5, entry 76). Besides the starting materials, also other reflections were observed (▼), that could not be assigned.

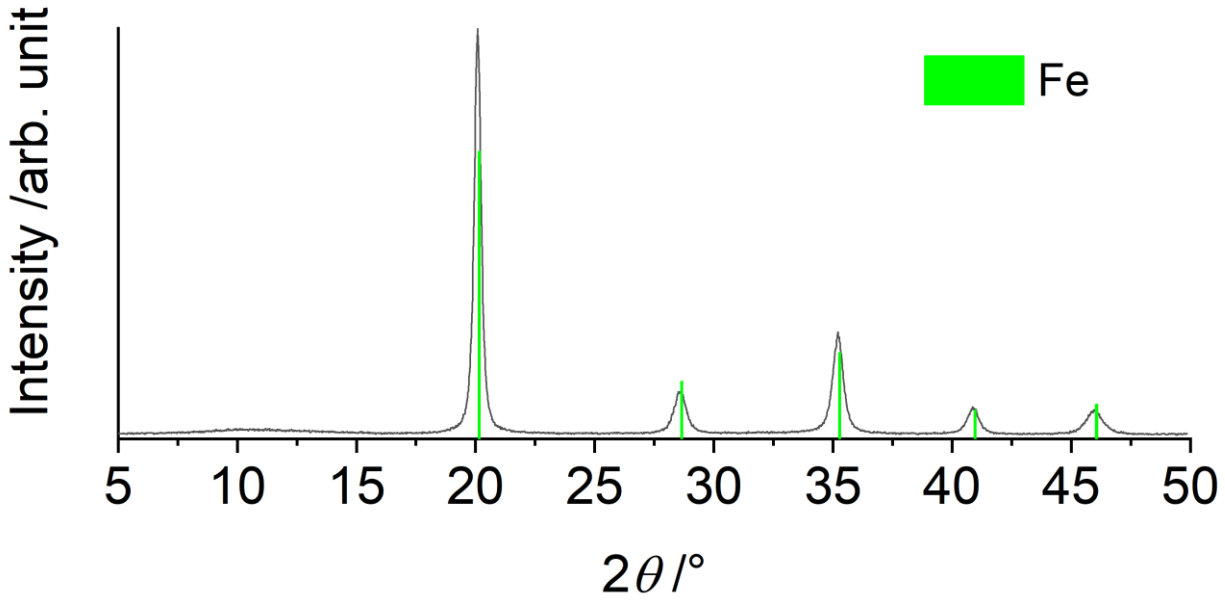

Fig. S52: PXRD of the catalyst powder after the continuous-flow reaction using CsOH · x H_2O and Fe (see table S5, entry 77). Only Fe is detected by X-ray diffraction. The concentration or crystallinity of the cesium phase(s) apparently was too low for detection.

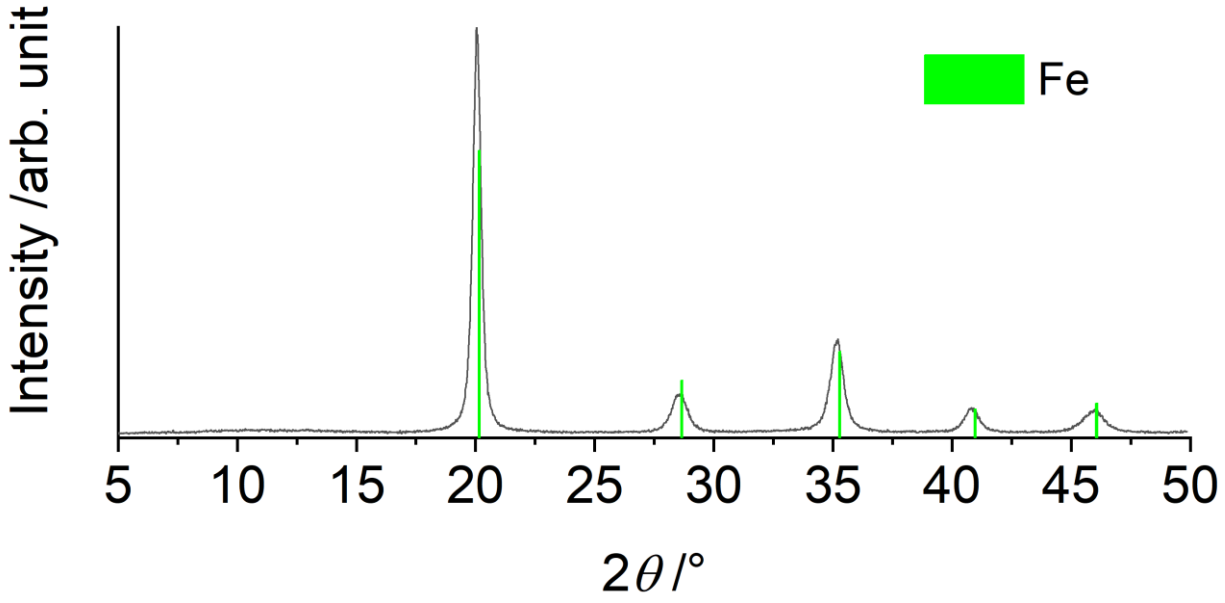

Fig. S53: PXRD of the catalyst powder after the continuous-flow reaction using CsH and Fe (see table S5, entry 78). Only Fe is detected by X-ray diffraction. The concentration or crystallinity of the cesium phase(s) apparently was too low for detection.

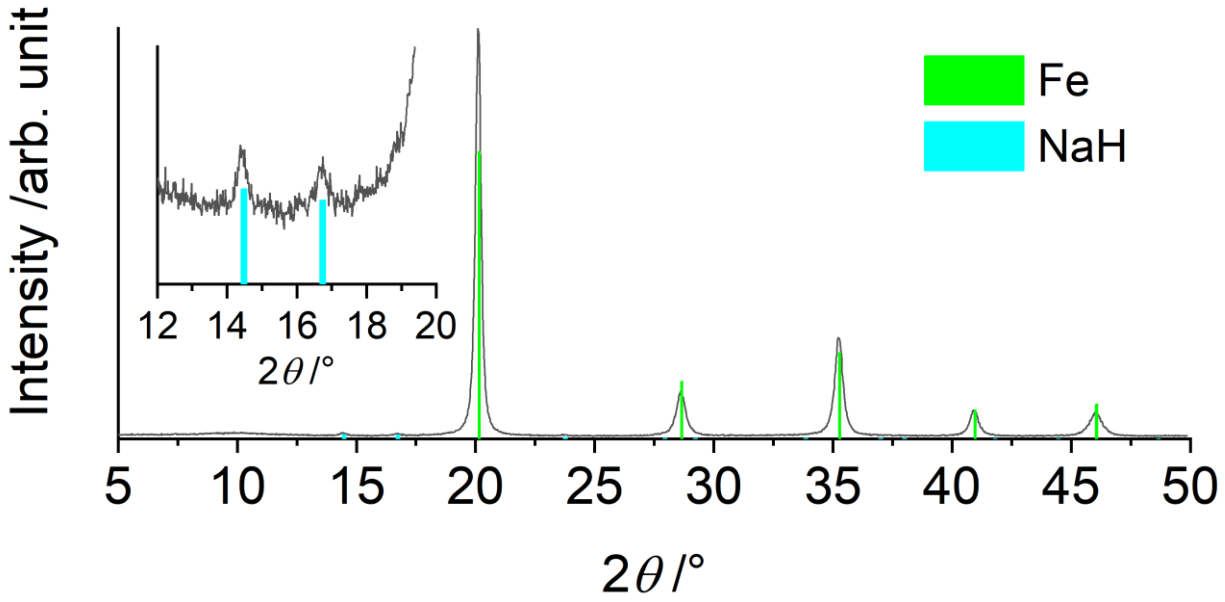

Fig. S54: PXRD of the catalyst powder after the continuous-flow reaction using NaH and Fe (see table S5, entry 79). Only the starting materials are detected by X-ray diffraction.

Table S6: Elemental analyses of selected materials. Iron starting material and selected products from the continuous-flow experiments were analyzed.

Sample description	C-content /%	H-content /%	N-content /%	Fe-content /%	Cs-content /%
Fe starting material	0.02	0.01	0.01	99.47	-
Table S5, entry 68[a]	0.11	0.07	0.58	93.45	4.76
Table S5, entry 67	0.07	0.05	0.50	93.00	4.19
Table S5, entry 78	0.11	0.06	0.61	92.31	4.41
Table S5, entry 77	0.10	0.04	0.08	94.13	4.70

[a] For this sample, also the Cr-content was determined. A value of 0.69 % indicates abrasion from the steel material.

References

[1] A. E. Abdel-Ghany, A. Mauger, H. Groult, K. Zaghib, C. M. Julien, *J. Power Sources* **2012**, *197*, 285-291.
[2] T. D. Perrine, H. Rapoport, *Anal. Chem.* **1948**, *20*, 635-636.
[3] R. Eckert, PhD thesis, Ruhr-Universität-Bochum (Germany), **2017**.
[4] P. J. Linstrom, W. G. Mallard, *NIST Chemistry WebBook, NIST Standard Reference Database Number 69*, National Institute of Standards and Technology, Gaithersburg MD, 20899.
[5] M. C. Biesinger, B. P. Payne, A. P. Grosvenor, L. W. M. Lau, A. R. Gerson, R. S. Smart, *Appl. Surf. Sci.* **2011**, *257*, 2717-2730.
[6] a) S. J. Yang, C. W. Bates, *Appl. Phys. Lett.* **1980**, *36*, 675-677; b) M. Ayyoob, M. S. Hegde, *Surf. Sci.* **1983**, *133*, 516-532.
[7] NIST X-ray Photoelectron Spectroscopy Database, *NIST Standard Reference Database Number 20*, National Institute of Standards and Technology, Gaithersburg MD, 20899, **2000**.
[8] S. Z. Andersen, V. Colic, S. Yang, J. A. Schwalbe, A. C. Nielander, J. M. McEnaney, K. Enemark-Rasmussen, J. G. Baker, A. R. Singh, B. A. Rohr, M. J. Statt, S. J. Blair, S. Mezzavilla, J. Kibsgaard, P. C. K. Vesborg, M. Cargnello, S. F. Bent, T. F. Jaramillo, I. E. L. Stephens, J. K. Norskov, I. Chorkendorff, *Nature* **2019**, *570*, 504-508.
[9] C. J. H. Jacobsen, S. Dahl, B. S. Clausen, S. Bahn, A. Logadottir, J. K. Norskov, *J. Am. Chem. Soc.* **2001**, *123*, 8404-8405.
[10] A. W. Tricker, K. L. Hebisch, M. Buchmann, Y. H. Liu, M. Rose, E. Stavitski, A. J. Medford, M. C. Hatzell, C. Sievers, *ACS Energy Lett.* **2020**, *5*, 3362-3367.
[11] P. K. Wang, F. Chang, W. B. Gao, J. P. Guo, G. T. Wu, T. He, P. Chen, *Nat. Chem.* **2017**, *9*, 64-70.
[12] M. Hattori, S. Iijima, T. Nakao, H. Hosono, M. Hara, *Nat. Commun.* **2020**, *11*, 2001, DOI: 10.1038/s41467-020-15868-8.

Author Contributions

S.R., M.F. and F.S. conceptualized the study. S.R. carried out the experiments, S.R., M.F. and F.S. analyzed and interpreted the results. S.R. wrote the original draft of the manuscript. M.F. and F.S. directed the study and reviewed and edited the original draft.